Global view of aerosol vertical distributions from CALIPSO lidar measurements and GOCART simulations: Regional and seasonal variations

Hongbin Yu[1,2], Mian Chin[2], David M. Winker[3], Ali H. Omar[3], Zhaoyan Liu[3,4], Chieko Kittaka[3,5], and Thomas Diehl[1,2]

[1] Goddard Earth Science and Technology Center, University of Maryland at Baltimore County, Baltimore, Maryland
[2] Laboratory for Atmospheres, NASA Goddard Space Flight Center, Greenbelt, Maryland
[3] NASA Langley Research Center, Hampton, Virginia
[4] National Institute of Aerospace, Hampton, Virginia
[5] Science System and Applications Inc., Hampton, Virginia

Correspondence
Hongbin Yu
NASA GSFC Code 613.2
Greenbelt, Maryland, 20771
Email: Hongbin.Yu@nasa.gov
Tel: (301) 614-6209 Fax: (301) 614-6307

Submitted to *the Journal of Geophysical Research – Atmospheres*
Special Issue *"Aerosol and Cloud Studies from CALIPSO and the A-train"*

July 23, 2009

Abstract: This study examines seasonal variations of the vertical distribution of aerosols through a statistical analysis of the Cloud-Aerosol Lidar and Infrared Pathfinder Satellite Observations (CALIPSO) lidar observations from June 2006 to November 2007. A data-screening scheme is developed to attain good quality data in cloud-free conditions and the polarization measurement is used to separate dust from non-dust aerosol. The CALIPSO aerosol observations are compared with aerosol simulations from the Goddard Chemistry Aerosol Radiation Transport (GOCART) model and aerosol optical depth measurements from the MODerate resolution Imaging Spectroradiometer (MODIS). The CALIPSO observations of geographical patterns and seasonal variations of aerosol optical depth (AOD) are generally consistent with GOCART simulations and MODIS retrievals especially near source regions, while the magnitude of AOD shows large discrepancies in most regions. Both the CALIPSO observation and GOCART model show that the aerosol extinction scale heights in major dust and smoke source regions are generally higher than that in industrial pollution source regions. The CALIPSO aerosol lidar ratio also generally agrees with GOCART model within 30% on regional scales. Major differences between satellite observations and GOCART model are identified, including (1) an underestimate of aerosol extinction by GOCART over the Indian sub-continent, (2) much larger aerosol extinction calculated by GOCART than observed by CALIPSO in dust source regions, (3) much weaker in magnitude and more concentrated in the lower atmosphere in CALIPSO observation than GOCART model and MODIS observation over transported areas in mid-latitudes, and (4) consistently lower aerosol scale height by CALIPSO observation than GOCART model. Possible factors contributing to these differences are discussed.

1. Introduction

Aerosol, also known as particulate matter (PM), can have significant impacts on air quality, weather, and climate [*Ostro et al.,* 1999; *McCormick and Ludwig,* 1967; *Twomey,* 1977; *Hansen et al.,* 1997]. Assessing these impacts requires an adequate, observational characterization of large temporal and spatial (both horizontal and vertical) variations of aerosol. The emerging capability of satellite remote sensing provides an unprecedented opportunity to advance the understanding of aerosol-air quality-climate linkages. Recent improvements in satellite remote sensing mainly aerosol optical depth (AOD) from passive sensors such as the Moderate resolution Imaging Spectroradiometer (MODIS) [*Remer et al.,* 2005; *Levy et al.,* 2007] and Multiangle Imaging Spectroradiometer (MISR) [*Kahn et al.,* 2005], have resulted in strong observational constraints for the aerosol direct effect on solar radiation in cloud-free conditions and at the top-of-atmosphere (TOA) [e.g., *Chen et al.,* 2009; *Remer and Kaufman,* 2006; *Yu et al.,* 2004, 2006]. Satellite AOD data have also been used to enhance the surface air quality monitoring networks for air quality forecast [e.g., *Al-Saadi et al.,* 2005] and to provide observation-based estimates of the long-range transport of aerosol [*Kaufman et al.,* 2005; *Yu et al.,* 2008]. However, passive sensors mainly provide total column quantities in clear scenes with little information on the vertical distribution of aerosols. As a result, current assessments of aerosol impacts on climate and air quality rely largely on model simulations of aerosol vertical distributions that differ by up to an order of magnitude among models [*Barrie et al.,* 2001; *Lohmann et al.,* 2001; *Textor et al.,* 2006], and remain very uncertain [*Corbin et al.,* 2002; *Schulz et al.,* 2006; *Yu et al.,* 2002].

Because of the recent launch of the Cloud-Aerosol Lidar and Infrared Pathfinder Satellite Observations (CALIPSO), the first-ever, continuous multi-year global aerosol profiling is emerging. This unique capability adds great value to aerosol and cloud research by complementing the increasingly sophisticated passive remote sensing of columnar aerosol (e.g., AOD). It also provides an opportunity to evaluate and constrain model simulations of aerosol vertical distributions that currently show large diversity. Objectives of this study are to: (1) analyze regional and seasonal variations of vertical distribution of aerosol extinction using the most recently available CALIPSO lidar observations, and (2) examine differences between CALIPSO observations and the Goddard Chemistry Aerosol Radiation Transport (GOCART) model simulations of aerosol vertical distributions. The real strength in CALIPSO is the vertical profile information more than the AOD, which is often less accurate than that retrieved by passive sensors. Therefore the significant results from this study come from CALIPSO-GOCART comparison of shapes of aerosol extinction profile. Through the statistical analysis of the first observed annual cycle of aerosol vertical distributions on a global scale and comprehensive comparison with the GOCART model, this study complements existing and ongoing validation efforts of CALIPSO measurements [e.g., *Kim et al.,* 2008; *Omar et al.,* 2009] and GOCART simulations [*Ginoux et al.,* 2001; *Chin et al.,* 2003] that are usually limited to specific regions and time periods. Different from the first global analysis of the occurring frequency of mineral dust from CALIPSO [*D. Liu et al.,* 2008], this work examines differences in the vertical distributions of aerosol extinction for both dust and non-dust aerosol between CALIPSO and GOCART.

The rest of paper is organized as follows. A brief description of CALIPSO lidar measurements and major uncertainties, and GOCART model simulations is given in section 2. Section 3 describes data analysis approaches, including various data screening and sampling techniques, and the broad categorization of aerosol type (dust and non-dust aerosol). In section 4, global patterns and regional variations of aerosol extinction profiles are presented and discussed on a seasonal basis through comparisons of CALIPSO measurements (June 2006 to November 2007) with GOCART simulations and MODIS retrievals of AOD. Major findings are summarized in Section 5.

2. Brief descriptions of satellite lidar measurements and model simulations

2.1. CALIPSO lidar measurements of aerosol vertical distributions

The CALIPSO mission was launched on April 28, 2006 in a 705 km sun-synchronous polar orbit with an equator-crossing time of about 1:30 pm and 1:30 am, local solar time, and a 16-day repeating cycle. It provides nearly global coverage between 82°N and 82°S. The primary instrument onboard the CALIPSO payload is the Cloud-Aerosol Lidar with Orthogonal Polarization (CALIOP), a two-wavelength, polarization lidar [*Winker et al.,* 2003]. Since June 13, 2006, CALIOP has been collecting almost continuously high-resolution profiles of the attenuated backscatter by aerosols and clouds at visible (532 nm) and near-infrared (1064 nm) wavelengths along with polarized backscatter in the visible channel [*Winker et al.,* 2007]. In the boundary layer and lower to middle free atmosphere (less than 8 km) where most atmospheric aerosols and clouds are found, CALIOP has a fundamental resolution of 333 m in the horizontal and 30 m in the vertical. Spatial averaging over different scales (e.g., 5, 20, or 80 km) is usually needed to obtain an improved signal-to-noise-ratio (SNR) for a reliable retrieval of aerosol profiles. The most frequent detection resolution for smoke, dust, clean continental, and polluted dust is 80 km [*Omar et al.,* 2009].

2.1.1. Cloud-aerosol discrimination

In the CALIOP data processing, features with enhanced signals relative to the clean atmosphere are first identified from the CALIOP measured attenuated backscatter that is calibrated at the TOA [*Vaughan et al.,* 2009; *Powell et al.,* 2009]. The sensitivity of feature detection increases with scale of spatial averaging because of the increased SNR and with altitude because of the smaller magnitude of the molecular scattering at higher altitude. The sensitivity is also better at night than during day because of additional background noise arising from sunlight. For aerosol layer product, theoretical estimate of minimum detectable backscatter coefficient is 2~4 x 10^{-4} $km^{-1}sr^{-1}$ in the troposphere [*Winker et al.,* 2009]. If a lidar ratio of 50 sr is assumed, the minimum detectable extinction coefficient is estimated to be 1~2 x10^{-2} km^{-1}. The identified features are then classified into aerosol and cloud using a cloud-aerosol discrimination (CAD) algorithm [*Liu et al.,* 2009] that is mainly based on multi-dimensional, altitude-dependent histograms of attenuated backscatter coefficient and its spectral dependence (e.g., color ratio) of aerosol and cloud [*Liu et al.,* 2004]. The existence of overlap in aerosol and cloud histograms complicates the CAD process in some cases. The level of confidence in the aerosol-cloud classification is reflected by a CAD score. The standard CAD scores range from -100 to 100, with a negative value to be associated with aerosol and a positive value with cloud. A larger absolute value of the CAD score indicates higher confidence of the feature classification.

2.1.2. Aerosol type classification

The CALIOP scene classification algorithm further associates the detected aerosol layer with one of six aerosol types (i.e., smoke, polluted continental, polluted dust, dust, clean continental,, and clean marine) using measurements of the integrated attenuated backscatter or IAB, volume depolarization ratio or VDR, and layer altitudes along with surface type [*Omar et al.,* 2009]. Based largely on a global cluster analysis of ground-based aerosol measurements [*Omar et al.,* 2005], the extinction-to-backscatter ratio or lidar ratio at 532 nm of 70, 70, 65, 40, 35, and 20 sr is prescribed for smoke, polluted continental, polluted dust, dust, clean continental, and clean marine, respectively [*Omar et al.,* 2009]. The determination of aerosol-type dependent lidar ratio serves to first retrieve the backscatter profile by correcting the attenuation of laser light and then to convert the retrieved backscatter to extinction linearly [*Young and Vaughan*, 2009]. The aerosol extinction thus increases with the lidar ratio nonlinearly.

2.1.3. Major uncertainties

Uncertainty associated with the determination of aerosol type and hence lidar ratio is one of major factors contributing to the uncertainty of CALIOP aerosol extinction retrieval. As discussed in *Winker et al.* [2009], if adequate spatial averaging has been taken to reduce the SNR errors to an insignificant level, the AOD error, $\delta\tau$, due to an error δS in lidar ratio (or fractional error $F_s = \delta S/S$) can be approximately estimated as follows and shown in **Figure 1**:

$$\delta\tau = 0.5(e^{2\tau} - 1)\frac{\delta S}{S} \qquad (1)$$

At small aerosol optical depth (e.g., AOD<0.1), the AOD fractional error ($\delta\tau/\tau$), can be approximately estimated as the fraction error of lidar ratio. However, with an increase of optical depth, the fractional error of lidar ratio is substantially amplified to result in a much higher AOD error. For example, the lidar ratio fractional error of 30% would result in an AOD fractional error of ~50% for AOD=0.5 and nearly 100% for AOD=1.

Uncertainties in the aerosol extinction retrieval can also arise from several other sources, such as the substantial attenuation of laser light by heavy aerosol layers and the ambiguity of cloud-aerosol discrimination in some cases. Because of the attenuation of light by overlying layers the space-borne lidar is difficult to detect aerosol layers near the surface, which biases aerosol extinction to the lower magnitude. Although the CAD algorithm works well in a majority of cases examined [*Liu et al*., 2009], several specific layer types can still be misclassified. In current CALIOP CAD algorithm, the use of global average probability density functions (PDFs) of optical properties for aerosol and cloud may be inadequate to capture the regional and seasonal variability of aerosol and cloud. This is particularly the case over or close to source regions where a dense dust or smoke layer may have a backscatter signal as strong as that for typical clouds. It is possible that such heavy dust or smoke might be misclassified as clouds [*Liu et al.,* 2009], which biases the aerosol extinction to a lower magnitude over or near the source regions. The layer height is also one of criteria used to distinguish aerosol from cloud so that features at high altitudes are more likely to be classified as clouds than as aerosol. If some aerosol layers (in particular dust) transported at high altitudes are classified as thin ice clouds, the CALIOP aerosol extinction would be underestimated somewhat, though the aerosols transported to the high altitudes are generally optically thin. On the other hand, optically thin clouds in the polar regions may be misclassified as aerosol [*Liu et al.,* 2009], which biases the aerosol extinction higher.

While extensive validation of CALIOP extinction profiles is still going on, several validation efforts have demonstrated that CALIOP has been quite successful in measuring aerosol vertical distributions. Comparisons of simultaneous CALIOP and ground-based lidar measurements over Korea show that the top and base heights of cloud and aerosol layers are generally in agreement within 0.10 km and the aerosol extinction profiles are generally in agreement within 30% in cloud-free conditions, and nighttime, semi-transparent cirrus cloud conditions [*Kim et al.,* 2008]. Comparisons with the High Spectral Resolution Lidar (HSRL) measurements from two field campaigns over the U.S., namely the CALIPSO And Twilight Zone (CATZ) and the Gulf of Mexico Atmospheric Composition and Climate Study (GoMACCS), show that the CALIOP average extinction biases higher by 0.003 km^{-1} (~20%) and 0.015 km^{-1} (~50%), respectively [*Omar et al.,* 2009].

2.2. GOCART model simulation of global aerosol distribution

The GOCART global model simulates the major aerosol types, including sulfate, mineral dust, black carbon, organic carbon, and sea salt. The assimilated meteorological fields from the Goddard Earth Observing System Data Assimilation System (GEOS DAS) Version 4 are used to drive the GOCART model. The spatial resolution of the GOCART model for this study is 2° latitude by 2.5° longitude in the horizontal and 30 layers in the vertical. Emissions from anthropogenic, biomass burning, biogenic, and volcanic sources and wind-blown dust and sea-salt are included. Other processes in GOCART are chemistry, convection, advection, boundary layer mixing, dry and wet deposition, gravitational settling, and hygroscopic growth of aerosol particles. Details of

GOCART model infrastructure and evaluation of its results against a variety of aerosol observations are documented in previous publications [*e.g., Chin et al.,* 2000a, 2000b, 2002, 2003, 2004, 2007, 2009; *Ginoux et al.,* 2001, 2004]. The GOCART model has contributed to several model intercomparisons and assessment reports [*e.g., IPCC,* 2001; *Yu et al.,* 2006, 2009; *Kinne et al.,* 2006; *Textor et al.,* 2006]. Note that the GOCART aerosol vertical distributions have been evaluated with measurements from lidar [*Ginoux et al.,* 2001] and aircraft [*Chin et al.,* 2003] over limited regions and seasons. There is a need for comprehensive evaluations of modeled vertical distributions of aerosol extinction using global observations over annual scale.

The GOCART aerosol optical properties, including extinction coefficient, backscatter coefficient, single-scattering albedo, and asymmetry factor, among others, are calculated from the Mie theory using prescribed size distributions, refractive indices, and hygroscopic properties of individual aerosol types that are taken from the Optical Properties for Aerosol and Cloud (OPAC) package [*Hess et al.*, 1998] and assuming external mixing of different aerosol types [*Chin et al.,* 2002, 2009]. It has been well known that the assumption of spherical particle in the Mie calculation can result in an overestimate of backscatter at 550 nm by a factor of ~2.5 for non-spherical dust [*e.g., Mattis et al.,* 2002; *Liu et al.*, 2002; *Dubovik et al.,* 2006]. In this study, the backscatter for spherical dust is empirically scaled to adjust this overestimate.

3. Data analysis approaches

3.1. Data sets and data screening

The major satellite data used in this study are CALIOP Level 2 Version 2.01 aerosol layer product from June 13, 2006 to November 30, 2007 that collects aerosol layers detected at horizontal resolution of 5, 20, and 80 km. The aerosol layer product provides the top and base of detected aerosol layer, and the layer integrated properties such as extinction AOD, attenuated backscatter (IAB), lidar ratio (S), volume depolarization ratio (VDR, including backscatter properties by both particle and air molecules), and CAD score, among others. Note that the CALIOP detected stratospheric features, which are also saved in the aerosol layer product, are excluded from our analysis, because these features have not been classified as either stratospheric aerosol or cloud. Thus our CALIOP analysis in this study deals with tropospheric aerosol only.

The analysis focuses on the CALIOP nighttime observations of aerosols in cloud-free conditions. Sunlight complicates the aerosol retrieval during daytime. As such the lidar observations at nighttime have higher accuracy than the daytime measurements. In this study the nominally "cloud-free" profiles are examined, including columns that are completely cloud-free or with the presence of high-level (e.g., cloud base higher than 7 km), optically thin (e.g., cloud optical depth less than 0.1) clouds. In the case of high-level thin clouds, the laser can still penetrate to sense aerosol layers underneath the cloud. The cloud-free conditions are determined by using the top, base, and optical depth of cloud layer from CALIOP 5-km cloud layer product (the same version as the aerosol layer product). The unique CALIOP capability of observing above-cloud aerosol is important to understanding the aerosol radiative forcing in cloudy conditions [*Chand et al.,* 2009], which is beyond the scope of this study.

Two further data screenings are applied to conduct statistical analysis with a large number of good-quality CALIOP measurements. One screening is to exclude detected aerosol layers that have low level of confidence in the cloud-aerosol discrimination. Without specific guideline on setting the CAD score threshold to screen the data, we include the aerosol data with CAD score between -50 and -100 in this analysis and examine sensitivity of results to the CAD threshold (**Figure 2**). Setting a more stringent CAD score criteria (e.g., excluding data with the CAD score >-90) reduces the number of sampled cloud-free data profiles and generally the grid and seasonal average AOD. About 60% of the AOD decrease of AOD is within 0.02 and ~80% within 0.04.The AOD decrease of more than 0.1 accounts for only about 3% of the data, which occurs mainly in the “dust belt” extending from the tropical Atlantic northeastward to the northwestern Pacific (roughly from 0° to 50°N and from 50°W to140°E) and in South America and South Africa in biomass burning seasons. Over these regions, the occurrence of dense dust or smoke would yield attenuated backscatter and its color ratio that are more likely to overlap with cloud histograms, resulting in a lower level of confidence of cloud-aerosol discrimination. On the other hand, relaxing the CAD score (e.g., excluding data with the CAD score >-20) increases the number of sampled cloud-free data profiles and generally the grid and seasonal average AOD. 90% of the AOD difference is within 0.02. The choice of CAD score threshold also has small effect on the aerosol scale height (within ± 200 m). Note that CAD>-20 represents some erroneously identified “pseudo-features” that are neither aerosol nor cloud, resulting from the noise of the signal, multiple scattering effects, and overestimate of the attenuation by the overlying layers [*Liu et al.,* 2009].

The other screening is to exclude aerosol layers where the retrieval algorithm has to adjust the initially selected lidar ratio that is based on the type and subtype of the aerosol layer being analyzed. Such adjustment usually occurs for complex features with high AOD that are vertically adjacent to or embedded in other features [*Omar et al.,* 2009]. In such cases, the retrieved optical depths and extinction profiles are generally not accurate and the associated uncertainty cannot be reasonably estimated [*Winker et al.,* 2009; *Young and Vaughan,* 2009].

3.2. Separation of dust and non-dust aerosol

The analysis is performed in the context of aerosol type by taking advantage of the polarization capability of CALIOP. The two polarization sensitive 532 nm receiver channels of CALIOP allow for the measurements of particulate depolarization ratio (PDR), a ratio of perpendicular component to parallel component of backscatter by aerosol particles. While non-spherical dust has a typical depolarization ratio of 0.1 to 0.4 [*Murayama et al.,* 2001; *Liu et al.,* 2002, 2008b; *Mattis et al.,* 2002; *Barnaba and Gobbi,* 2001], spherical particle has a near zero depolarization ratio. Therefore, PDR can be used to effectively distinguish non-spherical aerosol (e.g., dust, volcanic ash) from spherical aerosol (e.g., industrial pollution, biomass burning smoke, marine aerosol, and volcanic sulfate) [*Winker and Osborn*, 1992]. In the current release of CALIPSO products, PDR has not been retrieved. The variable instead available in the dataset is the VDR of aerosol layer, which reflects contributions from scattering of both molecules and particulates in a volume to the light polarization. Since the molecular scattering has a near-zero depolarization ratio of 0.0036 for CALIOP, the VDR of dust-laden air volume is smaller than the PDR of mineral dust [*Liu et al.*, 2008a]. The VDR approaches to PDR with high aerosol loading. As discussed in *D. Liu et al.* [2008], the desert dust can be largely separated from other types of aerosol (biomass burning smoke, continental and marine aerosol) by using a VDR threshold of 0.06. By following *D. Liu et al.* [2008], we broadly characterize each of CALIOP observed individual aerosol layers as "dust" when VDR is greater than 0.06 or as "non-dust" aerosol otherwise. The individual extinction profiles are aggregated separately into dust and non-dust aerosol to calculate respective regional and seasonal average profiles that are discussed in section 4. This simple VDR threshold approach is used to put the discussion of CALIOP measurements of aerosol extinction profiles in the context of aerosol type to some extent. In cases where dust mixes with other types of aerosols (e.g., pollution aerosol in India) in the same layer, it is hard to accurately compute the dust AOD using the threshold approach. Future efforts are needed to explore the use of PDR from upcoming CALIOP data releases to better partition the total extinction into dust and non-dust components.

3.3. Comparisons with GOCART and MODIS

The CALIOP data are compared with GOCART model simulations of three-dimensional aerosol distributions. For this purpose, GOCART aerosol simulation results (at 3hr interval) are sampled on the basis of the closest proximity in space and time to the CALIOP cloud free measurements. However, this sampling doesn't guarantee the exact match between GOCART and CALIOP, because of coarse resolutions (2.5°x2°) of GOCART model and near-zero swath of CALIPSO. We also use MODIS observations of AOD (Collection 5) [*Remer et al.,* 2005, 2008*; Levy et al.,* 2007] to evaluate CALIOP observations and GOCART simulations. To obtain sufficient data coverage, we use a combination of Terra and Aqua MODIS Level 3 daily 1°x1° data. When both Terra and Aqua aerosol retrievals are available over a grid, an average of them is used. The MODIS data are sampled from a grid encompassing the CALIOP cloud-free observation. Note that while MODIS aerosol measurements are performed during the daytime, CALIOP observations are sampled at night in this study. As CALIOP is the only means that measures nighttime aerosol, it is impossible to assess how the difference in time would complicate the intercomparisons. Here we assume that the difference in time is unlikely to cause significant differences in seasonal average AOD.

To facilitate the CALIOP-GOCART intercomparison of aerosol extinction (σ) profiles, we define aerosol scale height (H) as an above ground level (AGL) altitude below which 63% of total columnar integration of aerosol extinction (i.e., AOD) is present (following *Hayasaka et al.,* 2008), i.e.,

$$\int_0^H \sigma dz = (1-e^{-1}) \bullet AOD = 0.63 \bullet AOD \qquad (2)$$

In other words, the fractional AOD above H accounts for 37% of the total columnar AOD. A smaller scale height indicates that aerosol is more concentrated in the lower atmosphere. Although it does not reflect the detailed layer structures, H in conjunction with AOD provides a useful index for characterizing the aerosol vertical distribution on regional and global scales that involves large volumes of data, in particular for satellite-model and model-model intercomaprisons.

Our analysis focuses on (1) global patterns of aerosol optical depth and the scale height of aerosol extinction, and (2) regional and seasonal variations of the vertical distribution of aerosol extinction measured by CALIOP and modeled by GOCART.

Figure 3 illustrates 12 sections representing distinct aerosol regimes used for the regional analysis.

4. Results and discussion

4.1. Global distributions of aerosol optical depth and scale height

Because of its near-nadir view and the 16-day repeating cycle, a global view of aerosol can only be acquired by averaging the CALIOP cloud-free profiles collected over a period of time (e.g., a month or season) into grid boxes with a horizontal dimension on an order of degrees. In this study we calculate seasonal average cloud-free aerosol extinction and AOD over 5°x4° grids with a vertical resolution of 200 m by aggregating CALIOP individual shots of aerosol layers. **Figure 4** shows distributions of the number of the nominally cloud-free profiles detected by CALIOP in individual grids, including columns with detectable aerosol layers and clean columns where aerosol signal is too weak to be detected by CALIOP. In the latter case, aerosol extinction is set to 0 for this study. The detection of cloud-free profile generally occurs more frequently over land than over ocean, consistent with higher cloudiness over ocean. The number of the cloud-free profiles is also larger in arid and semi-arid areas than in other areas. Clearly, the number of CALIOP cloud-free aerosol samples is low in such regions as North Pacific, North Atlantic, part of tropical oceans, and Southern Oceans.

Figure 5 shows distributions of seasonal average cloud-free AOD at 532 nm observed by CALIOP and its comparisons with GOCART simulations and MODIS AOD retrievals at 550 nm for MAM 2007 and SON 2007. It appears that satellite observations (both CALIOP and MODIS) and the model give generally consistent spatial patterns of aerosol optical depth and its seasonal variations, with major continental source regions (dust, industrial pollution, and biomass burning) and the trans-Atlantic transport of Saharan dust being readily identified. Several major differences are evident on regional and continental scales. The CALIOP AOD is substantial lower than the GOCART simulation over North Africa and the western China where dust contribution is predominant. Over the Middle East and Indian subcontinent, on the other hand, the CALIOP AOD is higher than the GOCART simulation. Over West Europe, GOCART AOD is higher than CALIOP and MODIS observations. Over major tropical biomass burning regions (e.g., South America, southern Africa, and southeastern Asia in SON and central America in MAM), the CALIOP AOD is higher than the GOCART model simulation. One of other most pronounced differences is associated with the intercontinental transport of aerosols. Both MODIS and GOCART show that the trans-Pacific transport of aerosol from East Asia to North America is fairly strong in MAM, with AOD greater than 0.15 over the nearly entire mid-latitude North Pacific. However, the CALIOP observations show a much weaker trans-Pacific transport. Similar differences also exist for the trans-mid-Atlantic transport of aerosol from North America to West Europe. On the contrary, the westward transport of aerosol, mainly Saharan dust, by trade winds over tropical Atlantic is stronger and more extended from MODIS and CALIOP observations than the GOCART model. More quantitative comparisons of AOD on regional scales are discussed in the next section in conjunction with comparisons of aerosol extinction profiles.

Global patterns of the scale height for aerosol extinction provide a first order, global view of aerosol vertical distributions. **Figure 6** compares global distributions of the seasonal average aerosol scale height derived from CALIOP observations with the GOCART simulations for 2007. Clearly, the GOCART scale heights are consistently higher than the CALIOP observations. The differences are particularly large at the polar regions and northern hemispheric mid-latitudes away from the source regions where aerosols are generally transported from outside. The long-range transport of aerosol in these regions is usually associated with mid-latitude cyclones that can effectively lift pollution from the ABL to the upper troposphere [*Stohl et al.,* 2002]. The much lower CALIOP scale height than the GOCART model in these regions may result from the CALIOP sampling of cloud-free observations that may bias the scale height to low altitudes. CALIOP may miss to detect some optically thin layers in the FA because of the detection limit of lidar as discussed in 2.1, resulting in lower scale heights. It is also possible that GOCART model overestimates the vertical transport of aerosols and gives higher scale heights. Nevertheless, both CALIOP observation and GOCART model generally indicate higher scale heights over the dust belt and source regions of biomass burning (e.g., southern Africa and South America) than over industrial pollution source regions and over oceans.

4.2. Regional aerosol extinction profiles

While aerosol optical depth and scale height provide a useful, first order index of aerosol vertical distribution, detail structures of aerosol extinction can't be revealed. In the following, we discuss in greater detail the comparisons of seasonal average aerosol extinction and lidar ratio profiles between CALIOP observation and GOCART model over 12 selected regions. Seasonal and regional average lidar ratio S is calculated from individual values of lidar ratio weighted by the aerosol extinction. MODIS AOD is also included in the analysis to evaluate CALIOP retrieval and GOCART model. Although similar plots are made for all regions and seasons, for conciseness we only show plots in 8 representative sections, including eastern U.S. (EUS), eastern China (WUS), Indian subcontinent (IND), North Africa and Arabian peninsula (NAF), central Atlantic (CAT), northwestern Pacific (NWP), southern Africa (SAF) and southeast Asia (SEA) (see Figure 3). Our discussion also focuses on an annual cycle from December 2006 to November 2007 or some specific seasons with unique aerosol characterization in a region. Data from June 2006 to November 2006 are also discussed when significant year-to-year variations are revealed. In online supplementary material, we document similar plots in 4 other sections and tables that listed AOD and scale height in all sections and seasons.

4.2.1. Source regions of industrial pollution

Major source regions of industrial pollution include the eastern United States (EUS), West Europe (WEU), eastern China (ECN), and Indian subcontinent (IND), of which ECN and IND are also frequently influenced by mineral dust. **Figure 7** shows the vertical distributions of seasonal average aerosol extinction and lidar ratio, and comparisons of columnar total AOD between CALIOP (CAL), GOCART (GOC), and MODIS (MOD) over EUS. z is altitude above ground level (AGL), not mean sea level, throughout the paper. Also shown in the figure are aerosol scale height (H, km) and columnar total AOD (τ), with subscript C and G denoting CALIOP and GOCART, respectively. The aerosol extinction from CALIOP and GOCART in the atmospheric boundary layer (ABL, nominally 0-2km) agrees in the magnitude, with CALIOP extinction slightly larger than the GOCART counterpart. On the other hand, the CALIOP lidar ratio is generally smaller than GOCART simulations by 10-15 sr (15-20%) in JJA (June-July-August) and SON (September-October-November). In the middle to upper part of free atmosphere (FA) (generally higher than 4 km), however, the GOCART simulates an aerosol extinction of 0.003 – 0.018 km^{-1}, whereas CALIOP generally doesn't detect aerosol layers presumably because of the detection limit. This gives rise to the much higher scale heights (by 1-2.4 km) from GOCART model than from CALIOP observation, especially in MAM (March-April-May) than other seasons. While such differences in the FA are partly explained by the detection limit of CALIOP as discussed earlier, it is also possible that the model overestimates aerosol extinction in the FA. In terms of columnar integration of aerosol extinction or AOD over EUS, CALIOP agrees with GOCART in a range of -45% ~ +20 % but is 30-63% consistently smaller than MODIS AOD.

Figure 8 compares aerosol extinction profiles from CALIOP observation and GOCART model over eastern China. Except in DJF when CALIOP extinction is slightly higher than GOCART simulation in the ABL, the CALIOP observed extinction is smaller than the GOCART simulation near the surface and in the FA in other seasons, with the largest difference occurring in MAM and JJA. The aerosol layers (up to 0.04 km^{-1} in MAM) above 4 km as simulated by the GOCART model are not fully observed by CALIOP. As a result, the CALIOP scale height is about 800 m lower than the GOCART model. Again the differences may have resulted from both the possible model overestimate of upward transport and the CALIOP sensitivity limit. Both CALIOP and

GOCART suggest that the eastern China (mainly its northern part) is heavily influenced by dust in both seasons, with the dust fraction greater than 0.5 in MAM and DJF and relatively small (0.2~0.35) in JJA and SON. For aerosol lidar ratio, except in DJF when CALIOP agrees with GOCART, CALIOP lidar ratio is smaller than GOCART by 10-20 sr (15-30%) near the surface, with the difference decreasing with increasing altitude. This lidar ratio difference would explain a significant fraction of the AOD difference except in MAM, as can be inferred from Figure 1. In all seasons, the columnar AOD from MODIS is consistently larger than the CALIOP observation and GOCART simulation.

As shown in **Figure 9**, over the Indian subcontinent (IND) GOCART simulations of total aerosol extinction and AOD are consistently lower than satellite observations. The MODIS AOD can be up to a factor of 2 larger than the GOCART AOD. Except in JJA when CALIOP AOD is smaller than MODIS AOD by a factor of 2, CALIOP and MODIS AODs are generally quite consistent in other seasons. A comparison of GOCART AOD with measurements from AERONET at Kanpur site in India also shows that the GOCART model underestimates the AERONET AOD by more than a factor of 2 [*Chin et al.,* 2009]. All these comparisons appear to suggest that the GOCART model tends to underestimate the aerosol optical depth in this region. Despite the large CALIOP-GOCART difference in the magnitude of extinction, the general shape of vertical profiles is similar and the scale height of GOCART aerosol extinction is higher than CALIOP observation only by about 340 m on average. The figure also suggests that the CALIOP dust fraction is higher than the GOCART simulation by 0.24 to 0.4. This is qualitatively consistent with the lidar ratio (S) difference between CALIOP and GOCART, with the CALIOP S consistently smaller than the GOCART S by 10-20 sr

(15-30%). While the CALIOP observations apparently suggest that the underestimate of GOCART aerosol extinction results mainly from underestimate of dust extinction, comparisons against AERONET observations of spectral dependences of aerosol extinction (Ångström exponent) and single-scattering albedo at Kanpur site [*Chin et al.,* 2009] appear to suggest a slight underestimate of dust fraction by GOCART. With in mind that the current VDR threshold approach separating dust and non-dust aerosol may not be adequate for an accurate characterization of mixed dust and pollution aerosols, as mentioned in section 3.2, a better attribution of the underestimate of extinction to aerosol types requires a more robust separation of dust and non-dust aerosol from satellite measurements in the future.

4.2.2. Source regions of mineral dust

Dust is a predominant component of aerosol over North Africa and Arabian Peninsula (NAF) and the western China (WCN). **Figure 10** compares the aerosol extinction profiles from CALIOP and GOCART over NAF. Both CALIOP observation and GOCART model indicate that dust reaches the highest altitude in summer and the lowest altitude in winter, which is consistent with previous studies and is controlled by seasonal variations of turbulent mixing, atmospheric stability, and circulations [*Kalu,* 1979]. On the other hand, the top of aerosol layer observed by CALIOP is generally1-2 km lower than the GOCART simulation, due largely to the detection limit of lidar. The CALIOP observed aerosol extinction is also much smaller in magnitude with smaller vertical gradient in the lowest 2-3 km layer than the GOCART simulation. Overall the GOCART scale height is 0-0.5 km (0.26 km on average) higher than the CALIOP observation. CALIOP AOD over NAF is smaller than GOCART AOD by about 35% in JJA (both 2006 and 2007) but by more than a factor of 2 in other seasons. Similar CALIOP-GOCART differences exist over WCN (see online supplementary material).

Several uncertainties or issues associated with both model and satellite can result in the large satellite-model differences in the aerosol extinction. Generally, CALIOP gives the average lidar ratio of 40 - 45 sr in the region, which is about 5 - 15 sr (or 10-25%) smaller than GOCART simulated lidar ratio (50 - 54 sr). It appears that the CALIOP and GOCART dust lidar ratio shown here corresponds respectively to the lower end and higher end of observed dust lidar ratio range of 38-60 [*Tesche et al.,* 2009; *Muller et al.,* 2007; *De Tomasi et al.,* 2003, *Esselborn et al.,* 2009]. As the dust lidar ratio is sensitive to the shape of the non-spherical dust particles, chemical composition, and size distribution [*Barnaba and Gobbi,* 2001*; Liu et al.,* 2002], the observed wide range of lidar ratio may reflect the influence of dust from different source regions [*Esselborn et al.,* 2009].

While the CALIOP-GOCART lidar ratio difference discussed above is consistent with the extinction difference qualitatively, this relatively small difference of lidar ratio is unlikely to fully explain as much as a factor of 2 differences in the extinction and AOD. Several other factors would also contribute. For satellite measurements, it remains challenging to distinguish heavy dust loading from clouds, because of the usually large overlap of optical properties between them. As discussed in 2.1, over or close to source regions heavy dust might be misclassified as clouds and also attenuate the light substantially to make the extinction retrieval difficult in lower layers. Both issues bias the aerosol extinction to a lower magnitude and the latter also shifts the height of maximum extinction from near surface to a higher level (~ 500 m). From the perspective of model simulations, the GOCART model may have overestimated the source and atmospheric concentration of dust, as suggested by previous model evaluation and inter-comparison efforts. The global mean dust emission from GOCART is at the high end among 16 models that participated in the Aerosol Comparisons between Observations and Models (AeroCom) [*Textor et al.,* 2006]. Although comparisons of GOCART AOD with AERONET measurements show small positive bias (14%) of GOCART averaged over the NAF region [*Chin et al.,* 2009], the AERONET sites are mostly concentrated in the southern part of NAF region or at the coastal line in the northern NAF. So it is not clear how the GOCART model performs in the inland of the northern NAF because of lack of AERONET observations. As clearly shown in Figure 5, differences between the CALIOP observation and GOCART model are larger in northern NAF than in southern NAF.

4.2.3. Outflows downwind of major dust and industrial pollution source regions

The central Atlantic Ocean (CAT) is substantially influenced by dust from North Africa around a year and to some extent by biomass burning smoke from the tropical Africa in northern hemispheric winter. As shown in **Figure 11**, both CALIOP observations and GOCART simulations consistently indicate that dust is transported in both the ABL and free atmosphere, although the fraction of dust in the marine ABL is lower because of the existence of marine aerosol. Both the observation and model also show that dust layer is transported at higher altitudes in summer than in winter. This is consistent with previous observations. For example, the Saharan dust layer was observed above the trade winds inversion and up to 5-7 km in summer, but within the trade wind layer at altitudes below 1.5-3 km in winter [*Kalu et al.,* 1979; *Chiapello et al.,* 1997; *Liu et al.,* 2008b]. Unlike the large differences over the upwind source region (NAF) as discussed earlier, CALIOP and GOCART extinction profiles and AOD show much better agreement in this dust outflow region. Both CALIOP and GOCART AODs are generally smaller than MODIS AOD. Differences in lidar ratio are also small with the CALIOP values being <10 sr (or 10-20%) lower than the GOCART simulations.

On the contrary, substantial differences exist between CALIOP observations and GOCART simulations for both the East Asia outflows over the northwestern Pacific (NWP, **Figure 12**) and North America outflows over the mid-latitude North Atlantic. CALIOP AOD is lower than GOCART AOD (and also MODIS AOD) by more than a factor of 2, except in DJF (December-January-February) when the difference is much smaller. The large AOD differences result mainly from differences of aerosol extinction above the ABL. CALIOP rarely detects aerosol layers above 4 km, whereas GOCART simulations show consistent and considerable outflow of dust and non-dust aerosols throughout the FA. Although CALIOP did detect some aerosol layers between 4 and 6 km in MAM 2007, the observed magnitude of aerosol extinction was substantially smaller than the GOCART model. Seasonal average scale heights from the GOCART model range from 3.2–4.3 km, which is 1.2-2.3 km (1.85 km on average) higher than CALIOP observations. Aerosol scale heights as inferred from several ground-based lidar observations under cloud-free conditions in the region appear to agree better with CALIOP observations than with GOCART simulations. For example, *Hayasaka et al.* [2007] reported a wide range of scale height from 0.5 to 6 km over three Japanese sites in March-April-May 2005, of which about 80% are between 1.0 and 4.0 km and a smaller scale height generally corresponds to a larger AOD. *Nakajima et al.* [2007] reported the smaller scale height of 1-1.5 km during the same period. Observations over two Japanese sites in spring 2001 suggest that the scale height is 2-3 km for dust and 1-2 km for non-dust aerosol [*Shimizu et al.,* 2004]. Multi-year lidar observations over the Korean peninsula suggest that the scale height is about 2 km in spring, somewhat higher in summer and lower in winter and autumn [*Kim et al.,* 2007]. On the other hand, the aircraft measurements of dust during the ACE-Asia field experiment in spring 2001 shows a persistent feature of dust peaks at 4-5 km over the Yellow Sea and the Sea of Japan, which is well reproduced by GOCART model [*Chin et al.,* 2003].

The large differences between satellite observations and model simulations could result from several factors associated with both satellite and model. MODIS observation in this region is prone to cloud contamination [*Remer et al.,* 2005] and can be complicated by the presence of non-spherical dust in the region [*Chu et al.,* 2005]. GOCART model may have overestimated dust emissions and the aerosol transport to FA, as discussed earlier. From the perspective of CALIOP observations, there may be possible misclassifications in CALIOP aerosol sub-typing (and thus lidar ratio assignment) and aerosol-cloud discrimination. As discussed in 2.1, dust aerosol transported to the upper troposphere tends to be misclassified as thin cirrus clouds, resulting in somewhat underestimate of the aerosol extinction. As shown in the figure, the CALIOP lidar ratio in the marine ABL is generally much smaller than the GOCART simulation (in particular in summer). As described in *Omar et al.* [2009] (Figure 2), a feature is classified as polluted continental aerosol only when IAB is less than 0.01 and the depolarization is between 0.05 and 0.075. In other cases (depolarization ratio < 0.05

or IAB > 0.01), the feature is classified as marine aerosol. As marine aerosol and polluted continental aerosol have similar depolarization ratios, the simple threshold approach may not work well. For high aerosol loading with IAB>0.01 the feature is exclusively classified as marine aerosol, while the layer is more likely to be polluted continental aerosol. A statistical analysis shows that in the lowest 1km layer over the ocean, CALIOP characterizes aerosol features as marine aerosol at a respective frequency of 27% (DJF), 39% (MAM), 63% (JJA), and 55% (SON). The seasonality of marine aerosol detection frequency is consistent with that of lidar ratio discrepancy as shown in the figure. Given that marine aerosol has a lidar ratio of 20 sr at 532 nm that is smaller than that for continental pollution by a factor of ~3, a substantial underestimate of aerosol extinction can be resulted from a misclassification of polluted continental aerosol as marine aerosol in coastal areas where ABL pollution outflow occurs frequently.

The other probable factor is that CALIOP cloud-free observations discussed above may not be representative of GOCART simulations and MODIS observations. The outflows of pollution or pollution/dust mixture in NWP and NAT are usually associated with mid-latitude cyclones [*Stohl et al.,* 2002]. GOCART simulations represent averages over 2.5°x2° grids, including both clear and cloudy conditions. MODIS with a resolution of 500 m and nearly daily global coverage can sample areas close to cloud systems quite frequently. While CALIOP can sample in the vicinity of clouds because of its high spatial resolution, its single-nadir view and 16-day repeating cycle makes such sampling much less frequently. It is possible that the analysis of CALIOP cloud-free measurements as in this study (and ground-based lidar measurements too) may have missed some intense transport events associated with cloudy conditions. CALIOP does have a capability of detecting aerosols above the low-level clouds if high-level clouds are optically thin. Over NWP, CALIOP detected AOD above low-level clouds (with an average cloud top of about 1.5 km above the surface, for clouds with top lower than 4 km) is 0.07 for MAM, 0.046 for JJA, and 0.033 for DJF and SON. These above-cloud AODs differ from the cloud-free above-1.5 km AODs by less than 25% and are about 37-50% of cloud-free total columnar AOD. While these above-cloud AODs are significant in magnitude in comparison with the cloud-free values, it remains difficult to assess to what extent the exclusion of CALIOP observations in cloudy conditions contributes to the large differences between CALIOP and GOCART or MODIS because of lack of observations of aerosols below optically thick clouds.

4.2.4 Source regions of biomass burning smoke

The southern Africa (SAF) region defined in Figure 3 encompasses biomass burning sub-regions shifting with season: the Sahel region adjacent to the Sahara deserts with peak burning in DJF and the southern Africa with peak burning in JJA and SON. The region is also influenced by dust to some degree, because the predominant northerly to northeasterly over the Sahara deserts in the northern hemispheric winter can transport Saharan dust to the Sahel and the gulf of Guinea [*Kalu et al.,* 1979]. As shown in **Figure 13**, the lowest aerosol extinction occurs consistently in MAM from both CALIOP observation and GOCART model. GOCART simulates the highest extinction in DJF, which is about a factor of 2 larger than that in JJA and SON. On the other hand, CALIOP observations show no discernable difference between DJF, JJA and SON. As such the most pronounced CALIOP-GOCART differences occur in DJF. The GOCART AOD in

DJF is about 60% higher than measurements from both CALIOP and MODIS. The smoke layers between 4-6 km as calculated by the GOCART model are not observed by CALIOP. In other seasons, the model simulations of extinction and AOD agree with the satellite measurements within 10-30%. Another notable consistent feature in Figure 13 is a considerably large fraction of dust extinction in DJF and MAM, and a minimum dust fraction of less than 10% in JJA. The CALIOP observations suggest that the southward transport of Saharan dust imports AOD of 0.144 and 0.072 into the SAF region in DJF and MAM, respectively, which is more or less equivalent to the non-dust AOD in the region. For comparisons, GOCART simulations yield nearly the same dust AOD (i.e., 0.146 and 0.077 for DJF and MAM, respectively) and comparable percentile contribution of dust AOD (37% and 55%, respectively). The lower dust fraction (37%) of GOCART AOD in DJF results from much higher non-dust AOD calculated by the model than observed by CALIOP. For aerosol lidar ratio, CALIOP observations generally agree with the model simulations to within ±10 sr.

Figure 14 shows comparisons of aerosol extinction between CALIOP observation and GOCART model for SON, both 2006 and 2007, over South America (SAM). SON is peak biomass burning season in the region. As clearly shown in Figure 14, a significant amount of smoke aerosol is pumped above the ABL (over Amazon basin during the dry season, the convective ABL height in the afternoon reaches ~1 km over forest and ~1.6 km over pasture, *Fisch et al.,* 2004). The analysis is consistent with both in situ measurements [*Andreae et al.,* 2004] and the Geoscience Laser Altimeter System (GLAS) data [*Yu et al.,* 2007].

For SON 2006, the GOCART AOD of 0.12 is about 50% smaller than the CALIOP and MODIS observations (AOD=0.21 and 0.24, respectively). This may suggest possible underestimate of biomass burning emissions by GOCART model. On the other hand for SON 2007, the agreement between CALIOP and GOCART are reasonably good, except for the altitude of the largest aerosol extinction. While the CALIOP observation shows the largest extinction at 2 km, the GOCART model gives the largest extinction near the surface. One probable reason for this difference is that the attenuation of CALIOP signal would miss the detection of smoke near the surface, as discussed in section 2.1. For columnar AOD, both CALIOP and GOCART are nearly 50% smaller than the MODIS AOD of 0.46. The figure also shows significant interannual variability of biomass burning aerosol in the region. The biomass burning emissions of carbonaceous aerosol is about a factor of 3 higher in 2007 than 2006, as used in GOCART model. For both GOCART model and MODIS retrieval, AOD in 2006 is about half of that in 2007. Previous study also shows that MODIS AOD in 2006 is about a half of that in 2005 [*Koren et al.,* 2007]. The sharp decrease of biomass burning emission in 2006 is linked to the implementation of a tri-national policy on burning control in the region [*Koren et al.,* 2007]. However, CALIOP reveals a much smaller interannual variability, with AOD being 33% lower in 2006 than 2007, which would at least be linked partly to the uncertainty associated with laser attenuation by heavy smoke. The stronger attenuation of laser makes the smoke in the ABL less detectable by lidar in 2007, as corroborated by the elevation of height of maximum extinction from about 0.5 km in 2006 to 2 km in 2007.

5. Summary and conclusions

We have performed an analysis of three-dimensional distributions of seasonal average aerosol extinction at 532 nm by using CALIPSO lidar measurements in cloud-free nighttime conditions from June 2006 to November 2007. CALIOP measurements of aerosol extinction are compared with GOCART model simulations and MODIS AOD observations. Our analysis shows reasonably good agreements between satellite observations and model simulations, including:

1. In general, CALIOP observations of geographical patterns and seasonal variations of aerosol optical depth are consistent with GOCART simulations and MODIS retrievals, in particularly in source regions.
2. Both CALIOP observation and GOCART model show that the aerosol extinction scale heights in dust and smoke source regions are higher than that in industrial pollution source regions, though the scale height calculated by GOCART model is consistently higher than CALIOP observation.
3. Satellite observations and model simulations give a generally consistent characterization of both magnitude and altitude of trans-Atlantic transport of Saharan dust.
4. CALIOP observation and GOCART model agree in the estimated magnitude and seasonal variations of Saharan dust contribution to the aerosol extinction in the Sahel region.
5. For the aerosol lidar ratio, CALIOP observation generally agrees with GOCART model within 30%, except over Indian subcontinent and in

the marine ABL of northwestern Pacific and mid-latitude North Atlantic during some seasons. The best agreement occurs in biomass burning regions.

Several major differences between satellite observations and GOCART model are also identified, including:

1. Over Indian sub-continent, GOCART model tends to substantially underestimate the magnitude of aerosol extinction, as compared to MODIS and CALIOP retrievals and AERONET measurements. Although CALIOP observations seemingly suggest the underestimate resulting mainly from the dust aerosol, a robust attribution of uncertainties to aerosol types requires a better separation of dust from non-dust aerosol in the future.
2. In dust source regions, GOCART aerosol extinction is generally larger than CALIOP observation by a factor of 2 or more. This large difference could result from possible misclassification of heavy dust as clouds by CALIOP and/or overestimate of dust emissions by GOCART. With the addition of volume depolarization ratio to the aerosol PDFs of CALIOP CAD algorithm in the future, the dense dust layers can be identified.
3. For aerosol outflows from North America and East Asia, CALIOP observations under cloud-free conditions are much weaker in magnitude and much more concentrated in the lower atmosphere than that suggested by GOCART model and MODIS AOD observation. The

differences are likely to result from uncertainties associated with all datasets. MODIS AOD retrievals may have high bias resulting from cloud contamination and presence of non-spherical dust. The GOCART model may overestimate dust emissions and the transport of ABL aerosol to the FA. For CALIOP measurements, one probable reason is that current aerosol classification algorithm tends to misclassify ABL outflow of dense and spherical continental aerosol as marine aerosol and hence substantially underestimate extinction because of the assignment of too low lidar ratio. Another probable reason is that CALIOP's cloud-free observations, limited by the 16-day repeating cycle and high cloudiness in the regions, may have missed some important transport events associated with cloud systems, because mid-latitude cyclones are the most effective mechanism that pumps ABL aerosol to the free atmosphere for the subsequent intercontinental transport.

4. Over tropical biomass burning regions, GOCART model simulates higher aerosol loading in Sahel in winter but lower aerosol loading over South America in austral spring of 2006 than satellite observations. Year-to-year variations of biomass burning smoke over South America and southeastern Asia as revealed by CALIOP observations are generally much smaller than that suggested by the GOCART model and MODIS retrieval, which would be partly linked to more undetectable ABL smoke due to stronger laser attenuation in heavier smoke year.

Future efforts are needed to extend current analysis to above-cloud aerosol extinction profiles that are essential to estimating the aerosol direct radiative forcing in cloudy conditions. Possible daytime and nighttime differences in aerosol extinction profile need to be examined. In the future, a more robust separation of dust from non-dust aerosol is needed, such as the use of PDR to partition the extinction of detected aerosol layer into dust and non-dust components in dust-pollution mixture regions. This would be extremely helpful in effectively guiding the improvement of model simulations. Built on detail analysis of CALIOP and GOCART extinction profiles, much effort is needed to extend previous MODIS-GOCART integration framework [*Yu et al.*, 2003] by incorporating CALIOP measurements of vertical profiles and hence to achieve observation-based estimates of altitude-resolved aerosol direct radiative forcing.

Acknowledgements: This research was supported by the ACMAP and CALIPSO programs of NASA. We are grateful to Lorraine Remer for insightful comments. The CALIPSO data were obtained from the NASA Langley Research Center Atmospheric Sciences Data Center.

References

Al-Saadi, J., et al., Improving national air quality forecasts with satellite aerosol observations, *Bull. Am. Meteorol. Soc., 86,* 1249 – 1261, doi:10.1175/BAMS-86-9-1249, 2005.

Andreae, M. O., D. Rosenfeld, P., Artaxo, A. A., Costa, G. P. Frank, K. M. Longo, and M. A. F. Silva-Dias, Smoking rain clouds over the Amazon. *Science, 303,* 1337−1342, 2004.

Barnaba, F., and G. P., Gobbi, Lidar estimation of tropospheric aerosol extinction, surface area and volume: Maritime and desert dust cases, *J. Geophys. Res., 106,* 3005-3018, 2001.

Barrie, L. A., et al., A comparison of large-scale atmospheric sulphate aerosol models (COSAM): overview and highlights, *Tellus B, 53,* 615–645, 2001.

Chand D., R. Wood, T.L. Anderson, S.K. Satheesh, and R. J. Charlson, Satellite-derived direct radiative effect of aerosols dependent on cloud cover, *Nature Geoscience, 2,* 181-184, doi:10.1038/NGEO437, 2009.

Charlson, R. J. and M. J. Pilat, Climate: The influence of aerosols, *J. Appl. Meteorol., 8,* 1001-1002, 1969.

Chen, Y., Q. Li, R. Kahn, J. T. Randerson, and D. J. Diner, Quantifying aerosol direct radiative effect with MISR observations: 1. TOA albedo change by aerososl based on land surface types. *J. Geophys. Res., 114,* D02109, doi:10.1029/2008JD010754, 2009.

Chiapello, I. et al., Origins of African dust transported over the northeastern tropical Atlantic, *J. Geophys. Res., 102,* 13701-13709, 1997.

Chin, M., R. B. Rood, S.-J. Lin, J.-F. Muller, and A. M. Thompson, Atmospheric sulfur cycle simulated in the global model GOCART: Model description and global properties, *J. Geophys. Res., 105,* 24 671–24 687, 2000a.

Chin, M., et al., Atmospheric sulfur cycle in the global model GOCART: Comparison with field observations and regional budgets, *J. Geophys. Res., 105,* 24 689–24 712, 2000b.

Chin, M., et al., Tropospheric aerosol optical thickness from the GOCART model and comparisons with satellite and sunphotometer measurements, *J. Atmos. Sci., 59,* 461–483, 2002.

Chin, M., et al., A global model forecast for the ACE-Asia field experiment, *J. Geophys. Res., 108*, 8654, doi:10.1029/2003JD003642, 2003.

Chin, M., et al., Aerosol composition and distributions in the northern hemisphere during ACE-Asia: Results from global model, satellite observations, and surface sunphotometer measurements, *J. Geophys. Res., 109*, D23S90, doi:10.1029/2004JD004829, 2004.

Chin, M., T. Diehl, P. Ginoux, and W. Malm, Intercontinental transport of pollution and dust aerosols: implications for regional air quality, *Atmos. Chem. Phys., 7,* 5501– 5517, 2007.

Chin, M., T. Diehl, O. Dubovik, T. F. Eck, B. N. Holben, A. Sinuyk, and D. G. Streets, Light absorption by pollution, dust, and biomass burning aerosols: A global model study and evaluation with AERONET measurements, submitted to *Annales Geophysicae*, 2009.

Chu, D. A., et al., Evaluation of aerosol properties over ocean from Moderate Resolution Imaging Spectroradiometer (MODIS) during ACE-Asia, *J. Geophys. Res., 110,* D07308, doi:10.1029/2004JD005208, 2005.

Corbin, K. C., S. M. Kreidenweis, and T. H. Vonder Haar, Comparison of aerosol properties derived from Sun photometer data and ground-based chemical measurements, *Geophys. Res. Lett., 29,* 1363, doi:10.1029/2001GL014105, 2002.

De Tomasi, F., A. Blanco, and M. Perrone, Raman lidar monitoring of extinction and backscattering of African dust layers and dust caracterization, *Appl. Opt., 42,* 1699-1709, 2003.

Dubovik, O., et al., Application of spheroid models to account for aerosol particle nonsphericity in remote sensing of desert dust, *J. Geophys. Res., 111,* D11208, doi:10.1029/2005JD006619, 2006.

Esselborn, M., M. Wirth, A. Fix, B. Weinzierl, K. Rasp, M. Tesche, and A. Petzold, Spatial distribution and optical properties of Saharan dust observed by airborne high spectral resolution lidar during SAMUM 2006, *Tellus, 61B,* 131-143, 2009.

Ginoux, P., M. Chin, I. Tegen, J. Prospero, B. Holben, O. Dubovik, and S.-J. Lin, Sources and distributions of dust aerosols simulated with the GOCART model, *J. Geophys. Res., 106,* 20225–20273, 2001.

Ginoux, P., J. Prospero, O. Torres, and M. Chin, Long-term simulation of dust distribution with the GOCART model: Correlation with the North Atlantic Oscillation, *Environ. Modell. Softw., 19,* 113–128, 2004.

Hansen J., M. Sato, and R. Ruedy, Radiative forcing and climate response, *J. Geophys. Res., 102,* 6831-6864, 1997.

Hayasaka, T., et al., Vertical distribution and optical properties of aerosols observed over Japan during the Atmospheric Brown Clouds – East Asia Regional Experiment 2005, *J. Geophys. Res., 112,* D22S35, doi:10.1029/2006JD008086, 2007.

Hess, M., P. Koepke, and I. Schult, Optical properties of aerosols and clouds: The software package OPAC, *Bull. Am. Met. Soc., 79,* 831-844, 1998.

Intergovernmental Panel on Climate Change (IPCC), Climate Change 2001: *The Scientific Basis*, edited by: Houghton, J. T., Ding, Y., Nogua, M., et al., Cambridge University Press, New York, 2001.

Kahn, R. A., B. Gaitley, J. Martonchik, D. Diner, K. Crean, and B. Holben, MISR global aerosol optical depth validation based on two years of coincident AERONET observations. *J. Geophys. Res., 110,* doi: 10: 1029/2004JD004706, 2005.

Kalu, A.E., The African dust plume: Its characteristics and propagation across west Africa in winter, *SCOPE, 14,* 95-118, 1979.

Kaufman, Y. J., et al., Dust transport and deposition observed from the Terra-Moderate Resolution Imaging Spectroradiometer (MODIS) spacecraft over the Atlantic Ocean. *J. Geophys. Res., 110,* D10S12, doi: 10.1029/2003JDO04436, 2005.

Kim, S.-W., S.-C. Yoon, J. Kim, S.-Y. Kim, Seasonal and monthly variations of columnar aerosol optical properties over east Asa determined from multi-year MODIS, LIDAR, and AERONET Sun/sky radiometer measurements, *Atmos. Environ., 41,* 1634-1651, 2007.

Kim, S.-W., S. Berthier, J.-C. Raut, P. Chazette, E. Dulac, and S.-C. Yoon, Validation of aerosol and cloud layer structures from the space-borne lidar CALIOP using a ground-based lidar in Seoul, Korea, *Atmos. Chem. Phys.,* 8, 3705-3720, 2008.

Kinne S., M. Schulz, C. Textor, et al., An AeroCom initial assessment -- optical properties in aerosol component modules of global models. *Atmos. Chem. Phys., 6,*1815-1834, 2006.

Koren, I., L. A. Remer, and K. Longo, Reversal of trend of biomass burning in the Amazon. *Geophys. Res. Lett., 34,* L20404, doi:10.1029/2007GL031530, 2007.

Levy, R., L. A. Remer, S. Mattoo, E. Vermote, and Y. J. Kaufman, Second-generation algorithm for retrieving aerosol properties over land from MODIS spectral reflectance, *J. Geophys. Res., 112,* D13211, doi:10.1029/2006JD007811, 2007.

Liu, D., Z. Wang, Z. Liu, D. Winker, and C. Trepte, A height resolved global view of dust aerosols from the first year CALIPSO lidar measurements, *J. Geophys. Res., 113,* D16214, doi:10.1029/2007JD009776, 2008.

Liu, Z., N. Sugimoto, and T. Murayama, Extinction-to-backscatter ratio of Asian dust observed with high-spectral-resolution lidar and Raman lidar, *Appl. Opt., 41,* 2760-2767, doi:10.1364/AO.41.002760, 2002.

Liu, Z., et al., Use of probability distribution functions for discriminating between cloud and aerosol in lidar backscatter data, *J. Geophys. Res., 109,* D15202, doi:10.1029/2004JD004732, 2004.

Liu, Z., et al., Airborne dust distributions over the Tibetan Plateau and surrounding areas derived from the first year of CALIPSO lidar observations, *Atmos. Chem. Phys.*, *8***,** 5045-5060, 2008a.

Liu, Z., et al., CALIPSO lidar observations of the optical properties of Saharan dust: A case study of long-range transport, *J. Geophys. Res., 113,* D07207, doi:10.1029/2007JD008878, 2008b.

Liu, Z., et al., The CALIPSO Lidar Cloud and Aerosol Discrimination: Version 2 Algorithm and Initial Assessment of Performance, *J. Atmos. Oceanic Technol.,* 2009, *in press*

Lohmann, U., et al., Comparisons of the vertical distribution of sulfur species from models participated in COSAM exercise with observations, *Tellus, 53B,* 646-672, 2001.

Mattis, I., A. Ansmann, D. Muller, U. Wandinger, and D. Althausen, Dual-wavelength Raman lidar observations of the extinction-to-backscatter ratio of Saharan dust, *Geophys. Res. Lett., 29,* 1306, doi:10.1029/2002GL014721, 2002.

McCormick, R. A., and J. H. Ludwig, Climate modification by atmospheric aerosols, *Science, 156(3780),* 1358-1359, 1967.

Muller, D., A. Ansmann, I.Mattis, M. Tesche, U. Wandinger, D. Althausen, and G. Pisani, Aerosol-type-dependent lidar ratios observed with Raman lidar, *J. Geophys. Res., 112,* D16202, doi:10.1029/2006JD008292, 2007.

Murayama, T., et al., Ground-based network observation of Asian dust events of April 1998 in east Asia, *J. Geophys. Res., 106,* 18345-18360, 2001.

Nakajima, T., et al., Overview of the Atmospheric Brown Cloud East Asia Regional Experiment 2005 and a study of the aerosol direct radiative forcing in East Asia, *J. Geophys. Res., 112,* D24S91, doi:10.1029/2007JD009009, 2007.

Omar, A. H., J-G. Won, D. M. Winker, S-C. Yoon, O. Dubovik, and M. P. McCormick, Development of global aerosol models using cluster analysis of Aerosol Robotic Network (AERONET) measurements, *J. Geophys. Res., 110,* D10S14, doi:10.1029/2004JD004874, 2005.

Omar, A., D. Winker, C. Kittaka, M. Vaughan, Z. Liu, Y. Hu, C. Trepete, R. Rogers, R. Ferrare, R. Kuehn, and C. Hostetler, The CALIPSO automated aerosol classification and lidar ratio selection algorithm, submitted to *J. Atmos. Oceanic Technol.*, 2009.

Ostro, B., L. Chestnut, N. Vichit-Vadakan, and A. Laixuthai, The impact of particulate matter on daily mortality in Bangkok, Thailand. *J. Air and Waste Management Assoc., 49,* 100–107, 1999.

Powell, K.A., et al., CALIPSO lidar calibration algorithms: Part I – Nighttime 532 nm parallel channel and 532 nm perpendicular channel. *J. Atmos. Oceanic Technol.,* 2009, in press.

Remer, L. A., et al., The MODIS aerosol algorithm, products, and validation, *J. Atmos. Sci., 62,* 947– 973, doi:10.1175/JAS3385.1, 2005.

Remer, L. A., and Y. J. Kaufman, Aerosol direct radiative effect at the top of the atmosphere over cloud free ocean derived from four years of MODIS data. *Atmos. Chem. Phys., 6,* 237-253, 2006.

Remer, L. A., et al., An emerging aerosol climatology from the MODIS satellite sensors, *J. Geophys. Res., 113,* D14S07, doi:10.1029/2007JD009661, 2008.

Schulz, M., et al., Radiative forcing by aerosols as derived from the AeroCom present-day and pre-industrial simulations, *Atmos. Chem. Phys., 6,* 5225-5246, 2006.

Shimizu, A., et al., Continuous observations of Asian dust and other aerosols by polarization lidars in China and Japan during ACE-Asia, *J. Geophys. Res., 109,* D19S17, doi:10.1029/2002JD003253, 2004.

Stohl, A., et al., On the pathways and timescales of intercontinental air pollution transport, *J. Geophys. Res., 107*, 4684, 2002.

Tesche, M., et al., Verticalprofiles of Saharan dust with Raman lidars and airborne HSRL in southern Morocco during SAMUM, *Tellus, 61B,* 144-164, 2009.

Textor, C., et al., Analysis and quantification of the diversities of aerosol life cycles within AeroCom, *Atmos. Chem. Phys., 6,* 1777–1813, 2006.

Twomey, S., The influence of pollution on the shortwave albedo of clouds. *J. Atmos. Sci. 34,* 1149-1152, 1977.

Vaughan, M., et al., Fully automated analysis of space-based ldiar data: an overview of the CALIPSO retrieval algorithms and data products, *Proc. SPIE Int. Soc. Opt. Eng., 5575,* 16-30, doi:10.1117/12.572024, 2004.

Winker, D.M. and M.T. Osborn, Preliminary Analysis of Observations of the Pinatubo Volcanic Plume with a Polarization-Sensitive Lidar, *Geophys. Res. Letts. 19,* 171-174, 1992.

Winker, D.M., J. Pelon, and M.P. McCormick, The CALIPSO mission: Spaceborne lidar for observations of aerosols and clouds. *Proc. SPIE*, 4893, 1-11, 2003.

Winker, D., W.H. Hunt, and M.J. McGill, Initial performance assessment of CALIOP, *Geophys. Res. Lett., 34,* L19803, doi:10.1029/2007GL030135, 2007.

Winker, D.M., M.A. Vaughan, A. Omar, Y. Hu, K.A. Powell, Z. Liu, W.H. Hunt, and S.A. Young, Overview of the CALIPSO mission and CALIOP data processing algorithms. *J. Atmos. Oceanic Technol.*, 2009, in press.

Young, S.A., and M.A. Vaughan, The retrieval of profiles of particulate extinction from Cloud Aerosol Lidar Infrared Pathfinder Satellite Observations (CALIPSO) lidar data: Algorithm description, *J. Atmos. Oceanic Technol.,* 2009, in press.

Yu, H., S.C. Liu, and R.E. Dickinson, Radiative effects of aerosols on the evolution of the atmospheric boundary layer, *J. Geophys. Res., 107,* 4142, doi:10.1029/2001JD000754, 2002.

Yu, H., R. E. Dickinson, M. Chin, et al., Annual cycle of global distributions of aerosol optical depth from integration of MODIS retrievals and GOCART model simulations, *J. Geophys. Res., 108,* 4128, doi:10.1029/2002JD002717, 2003.

Yu, H., R.E. Dickinson, M. Chin, et al., The direct radiative effect of aerosols as determined from a combination of MODIS retrievals and GOCART simulations, *J. Geophys. Res.*, *109,* D03206, doi:10.1029/2003JD003914, 2004.

Yu, H., Y. J. Kaufman, M. Chin, et al., A review of measurement-based assessments of the aerosol direct radiative effect and forcing, *Atmos. Chem. Phys., 6,* 613– 666, 2006.

Yu, H., R. Fu, R. E. Dickinson, Y. Zhang, M. Chen, and H. Wang, Interannual variability of smoke and warm cloud relationships in the Amazon as inferred from MODIS retrievals. *Remote Sens. Environ.*, *111,* 435-449, 2007.

Yu, H., L.A. Remer, M. Chin, H. Bian, R. Kleidman, and T. Diehl, A satellite-based assessment of trans-Pacific transport of pollution aerosol, *J. Geophys. Res., 113,* D14S12, doi:10.1029/2007JD009349, 2008.

Yu, H., P. K. Quinn, G. Feingold, L. A. Remer, R. A. Kahn, M. Chin, and S. E. Schwartz, Remote Sensing and *In Situ* Measurements of Aerosol Properties, Burdens, and Radiative Forcing, in *Atmospheric Aerosol Properties and Climate Impacts,* A Report by the U.S. Climate Change Science Program and the Subcommittee on Global Change Research. [Mian Chin, Ralph A. Kahn, and Stephen E. Schwartz (eds.)]. National Aeronautics and Space Administration, Washington, D.C., USA, 2009.

Figure Captions

Figure 1: Fractional error of aerosol optical depth, $\delta\tau/\tau$, resulting from fractional error of lidar ratio ($Fs=\delta S/S$) (following analysis of Winker et al, 2009).

Figure 2: Cumulative frequency of AOD difference [d(AOD)] due to using different thresholds of CAD score to screen the CALIOP data, with blue line representing difference between CAD<-90 and CAD<-50 and red line for difference between CAD<-20 and CAD<-50. The AOD differences are calculated from grid (5°x4°) and seasonal average CALIOP AOD on a global scale and over the 18-month period from June 2006 to November 2007.

Figure 3: 12 sections selected for regional analysis in this study, covering source regions of dust (NAF and WCN), biomass burning smoke (SAF, SAM, and SEA), and industrial pollution (EUS, and WEU, ECN, and IND), as well as outflow regions downwind of major dust and industrial pollution sources (CAT, NAT, and NWP).

Figure 4: Distributions of the number of nominally cloud-free profiles sensed by CALIOP within each 5°x4° grid during MAM 2007 (top) and SON 2007 (bottom).

Figure 5: Distributions of seasonal average AOD in cloud-free conditions in (a) MAM 2007, and (b) SON 2007. GOCART simulations and MODIS retrievals are sampled along CALIPSO tracks.

Figure 6: Global patterns of seasonal average scale height (km, above the ground level) of aerosol extinction in cloud-free conditions derived from CALIOP observations and GOCART simulations.

Figure 7: Profiles of seasonal average aerosol extinction coefficient (km^{-1}) and lidar ratio (sr) from CALIOP observation and GOCART model, as well as comparisons of columnar AOD between CALIOP (CAL), GOCART (GOC), and MODIS (MOD) over the eastern

U.S. (EUS). Values of aerosol scale height (H) and optical depth (τ) are listed in the extinction profile plots, with subscript C and G representing CALIOP and GOCART respectively. Orange and blue shaded area in extinction profile and AOD plots represents contribution of dust and non-dust aerosol, respectively.

Figure 8: same as Figure 7, but over the eastern China (ECN).

Figure 9: same as Figure 7, but over the Indian subcontinent (IND).

Figure 10: same as Figure 7, but over North Africa and Arabian Peninsula (NAF). Note that because of missing MODIS retrievals over deserts, MODIS AOD is not directly comparable to CALIOP and GOCART averages.

Figure 11: same as Figure 7, but over the central Atlantic (CAT).

Figure 12: same as Figure 7, but over the northwestern Pacific (NWP).

Figure 13: same as Figure 7, but over the southern Africa (SAF).

Figure 14: same as Figure 7, but over South America (SAM) and for SON 2006 and SON 2007.

Figures

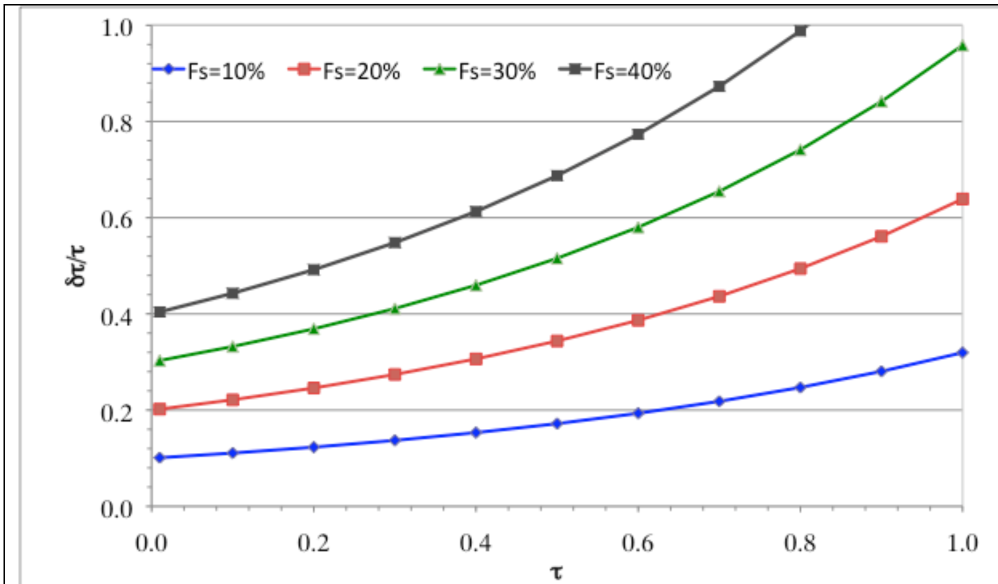

Figure 1: Fractional error of aerosol optical depth, δτ/τ, resulting from fractional error of lidar ratio (Fs=δS/S) (following analysis of Winker et al, 2009).

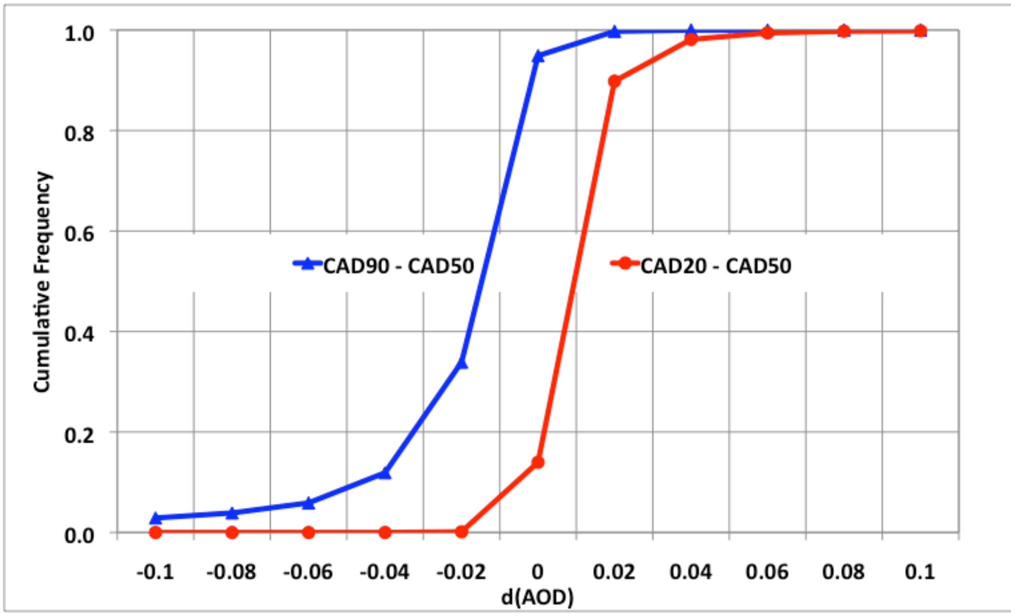

Figure 2: Cumulative frequency of AOD difference [d(AOD)] due to using different thresholds of CAD score to screen the CALIOP data, with blue line representing difference between CAD<-90 and CAD<-50 and red line for difference between CAD<-20 and CAD<-50. The AOD differences are calculated from grid (5°x4°) and seasonal average CALIOP AOD on a global scale and over the 18-month period from June 2006 to November 2007.

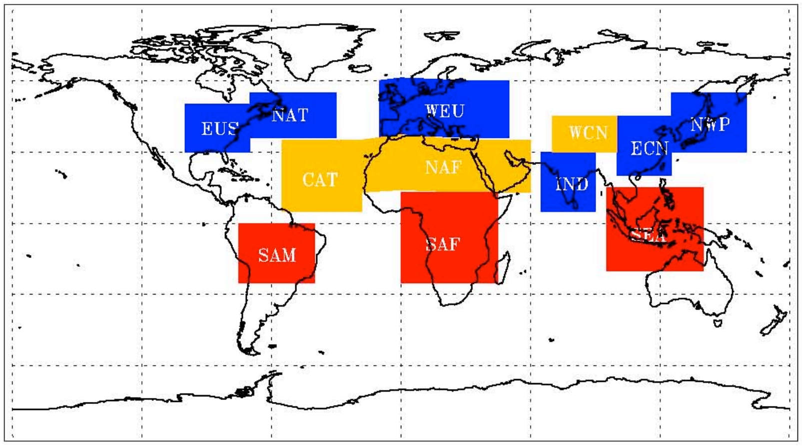

Figure 3: 12 sections selected for regional analysis in this study, covering source regions of dust (NAF and WCN), biomass burning smoke (SAF, SAM, and SEA), and industrial pollution (EUS, and WEU, ECN, and IND), as well as outflow regions downwind of major dust and industrial pollution sources (CAT, NAT, and NWP).

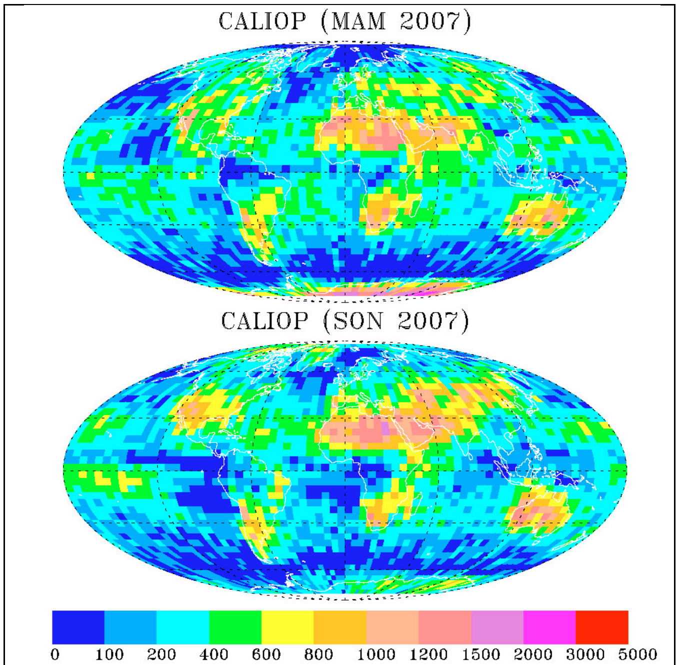

Figure 4: Distributions of the number of nominally cloud-free profiles sensed by CALIOP within each 5°x4° grid during MAM 2007 (top) and SON 2007 (bottom).

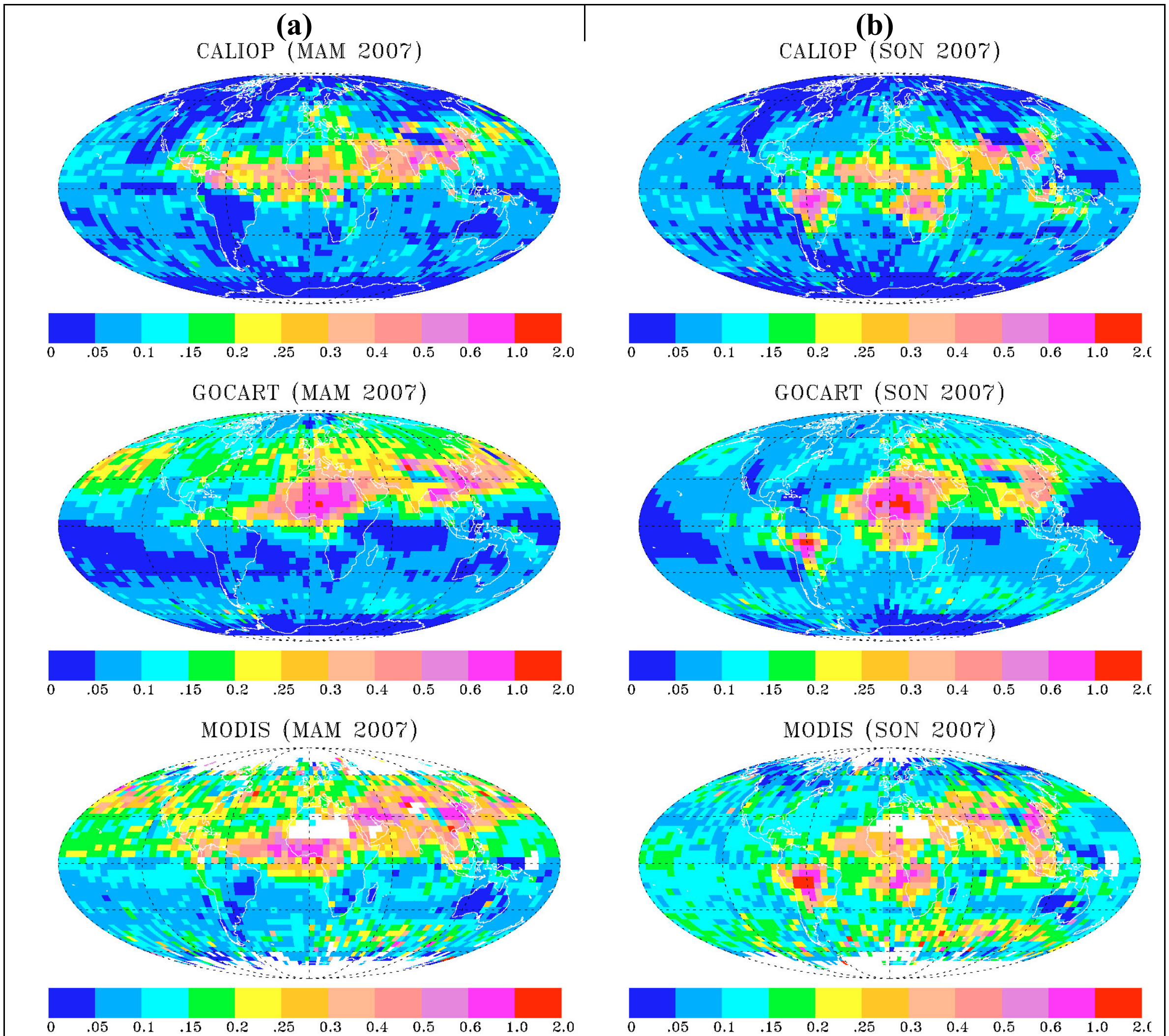

Figure 5: Distributions of seasonal average AOD in cloud-free conditions in (a) MAM 2007, and (b) SON 2007. GOCART simulations and MODIS retrievals are sampled along CALIPSO tracks.

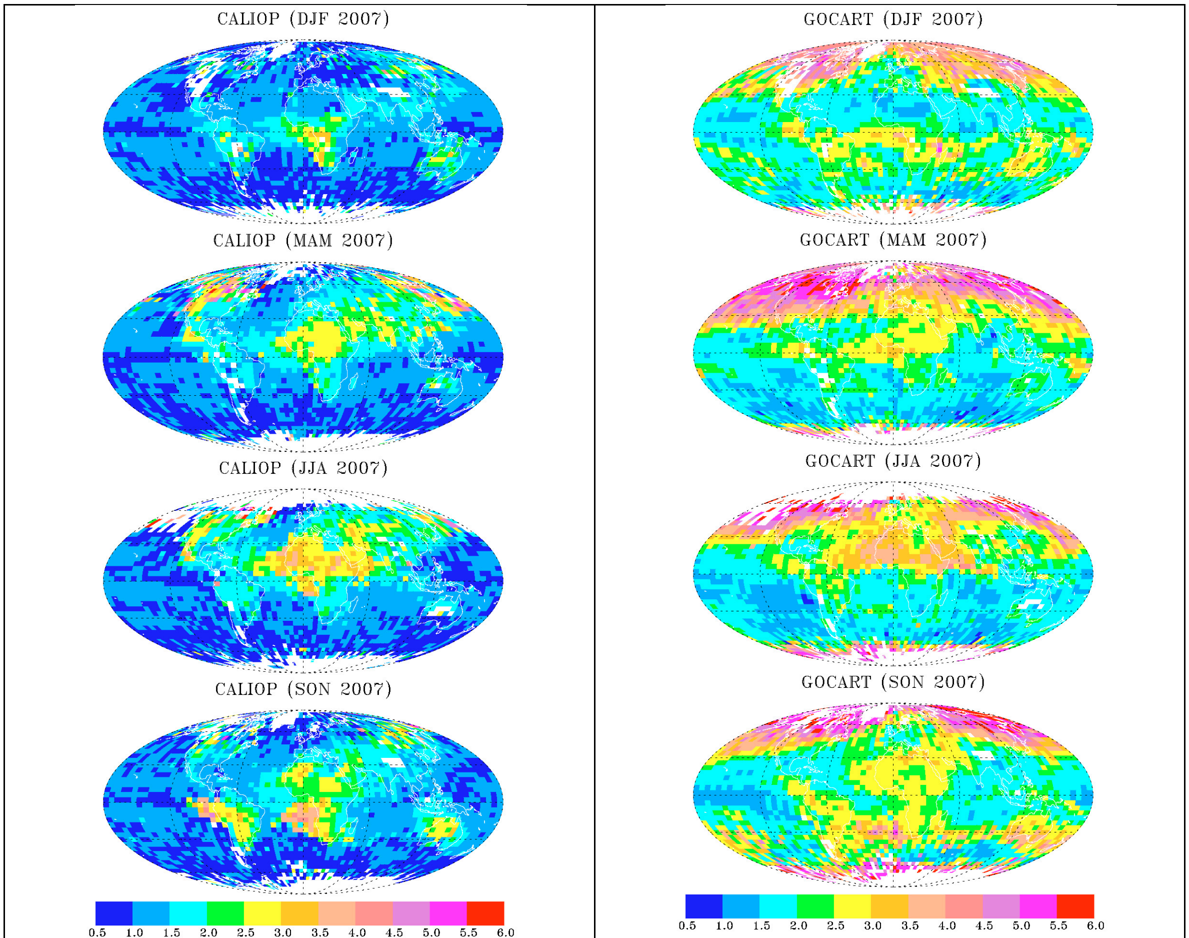

Figure 6: Global patterns of seasonal average scale height (km, above the ground level) of aerosol extinction in cloud-free conditions derived from CALIOP observations (left) and GOCART simulations (right).

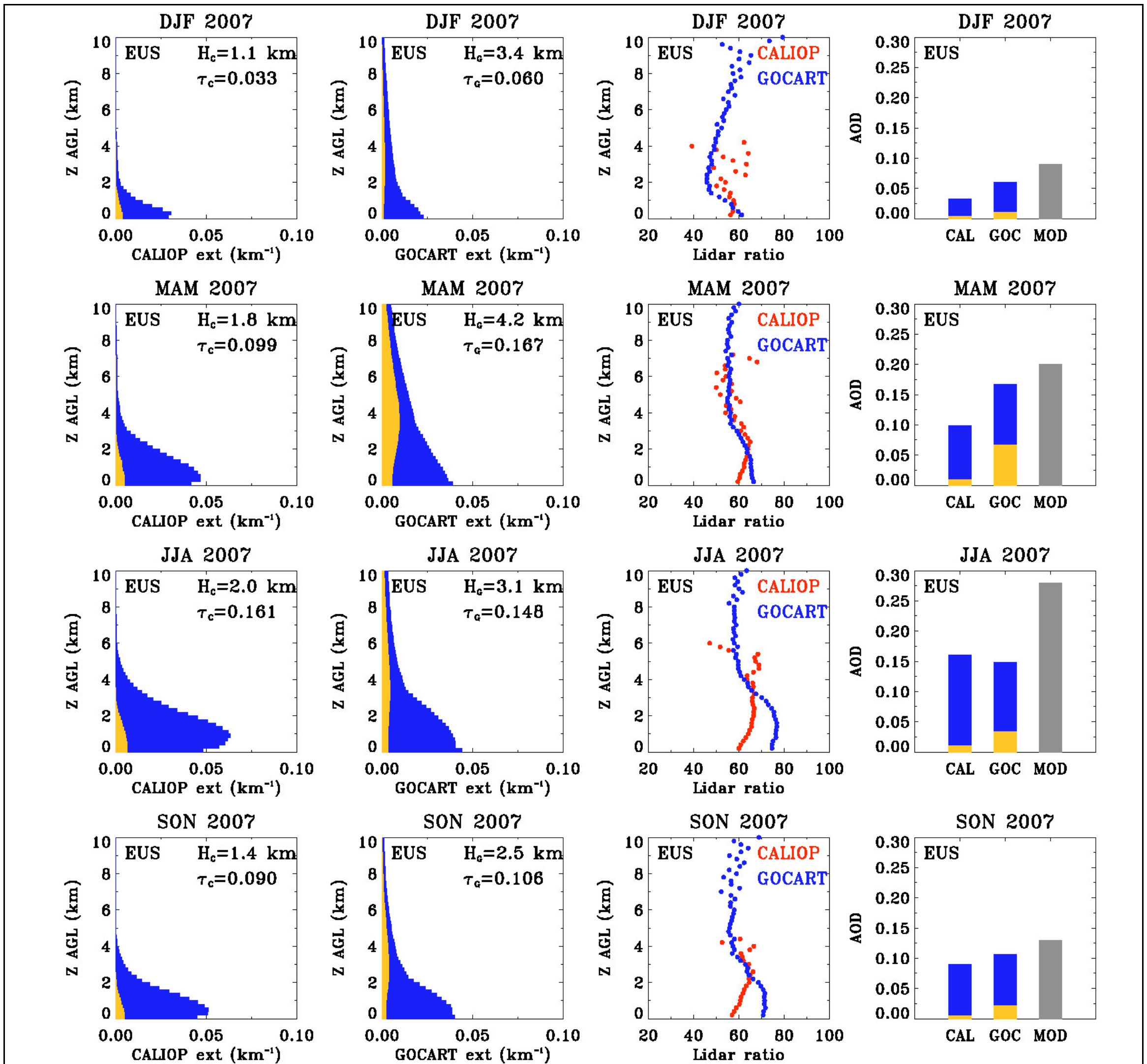

Figure 7: Profiles of seasonal average aerosol extinction coefficient (km^{-1}) and lidar ratio (sr) from CALIOP observation and GOCART model, as well as comparisons of columnar AOD between CALIOP (CAL), GOCART (GOC), and MODIS (MOD) over the eastern U.S. (EUS). Values of aerosol scale height (H) and optical depth (τ) are listed in the extinction profile plots, with subscript C and G representing CALIOP and GOCART respectively. Orange and blue shaded area in extinction profile and AOD plots represents contribution of dust and non-dust aerosol, respectively.

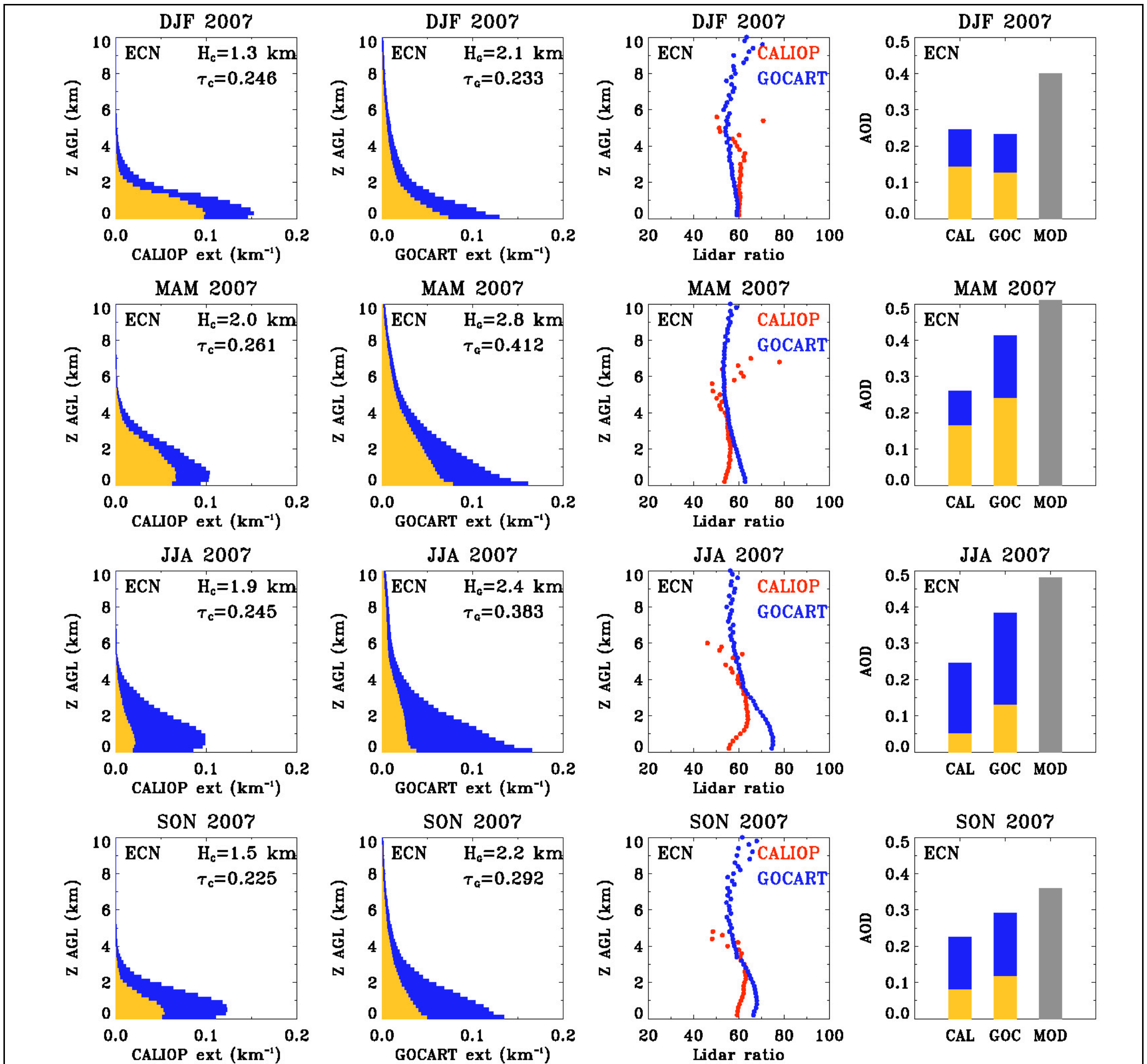

Figure 8: same as Figure 7, but over the eastern China (ECN).

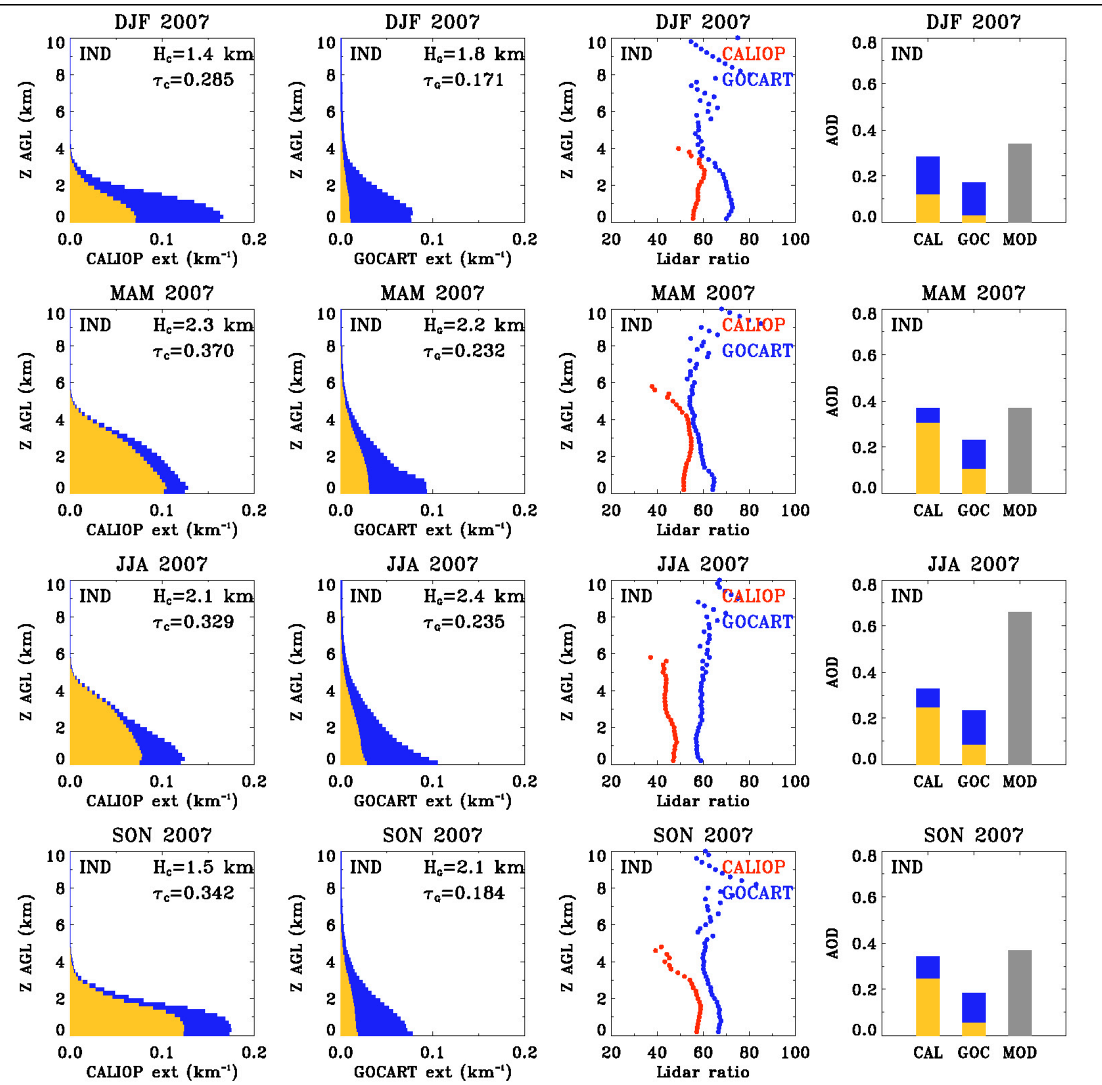

Figure 9: same as Figure 7, but over the Indian subcontinent (IND).

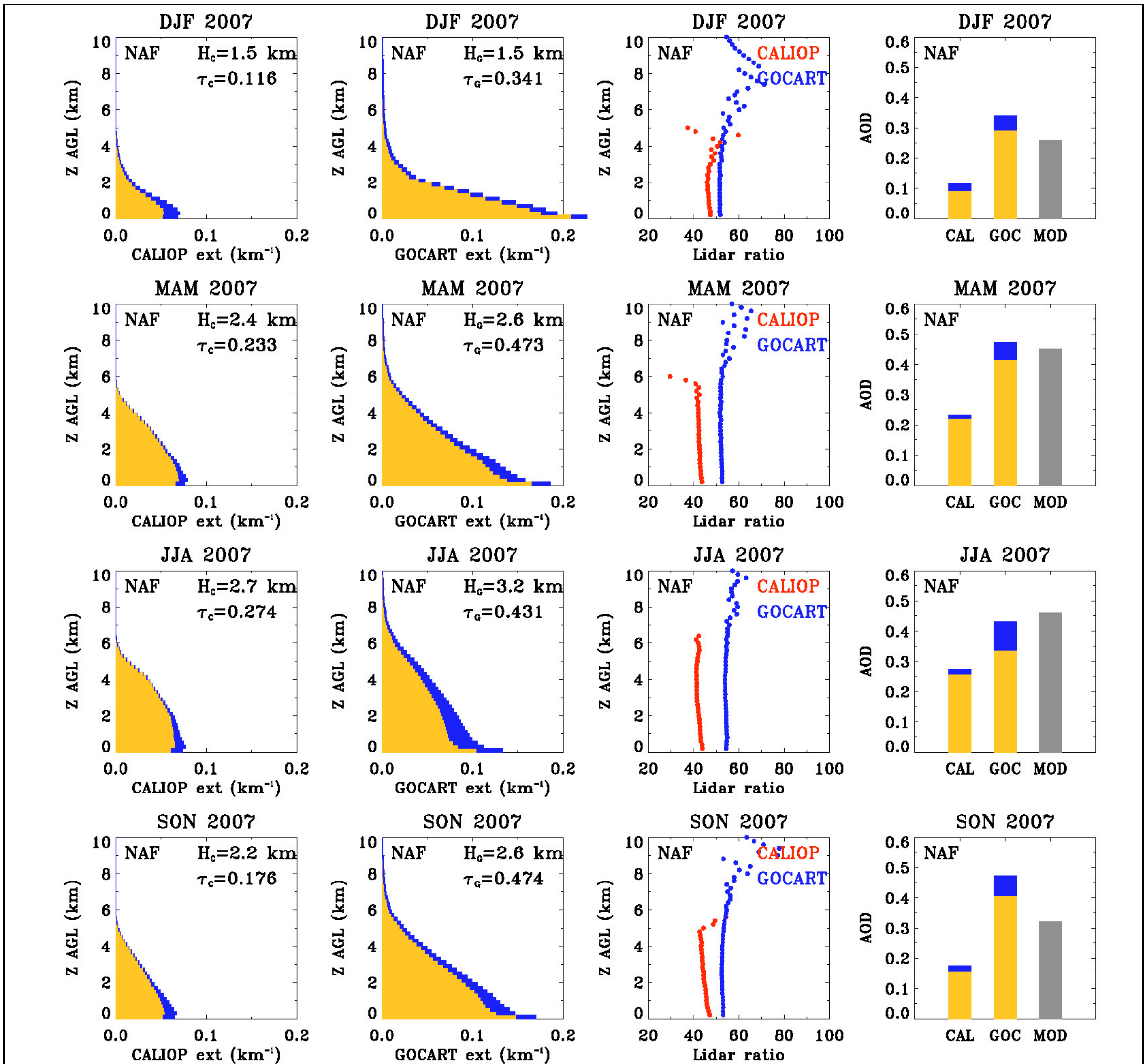

Figure 10: same as Figure 7, but over North Africa and Arabian Peninsula (NAF). Note that because of missing MODIS retrievals over deserts, MODIS AOD is not directly comparable to CALIOP and GOCART averages.

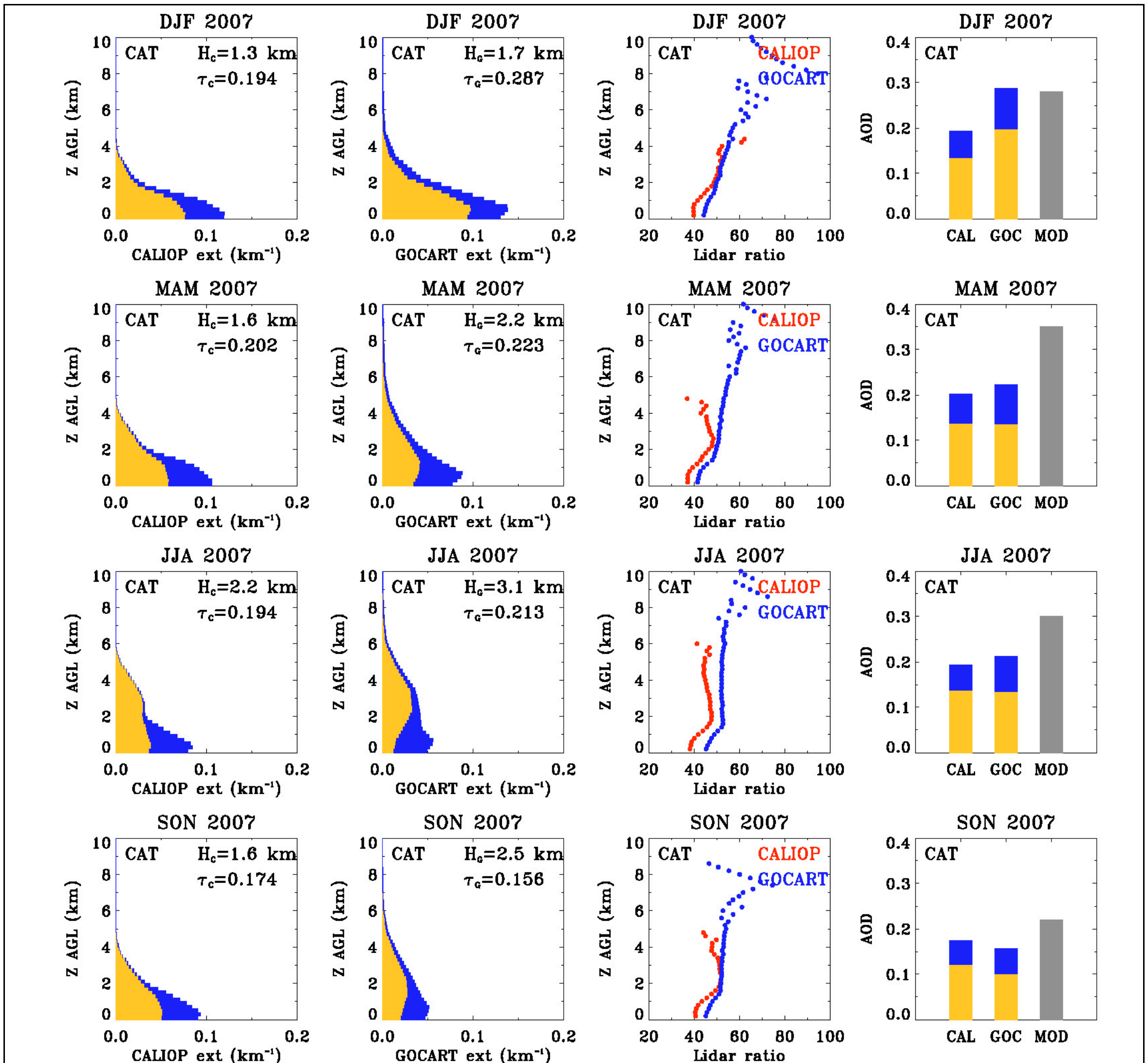

Figure 11: same as Figure 7, but over the central Atlantic (CAT).

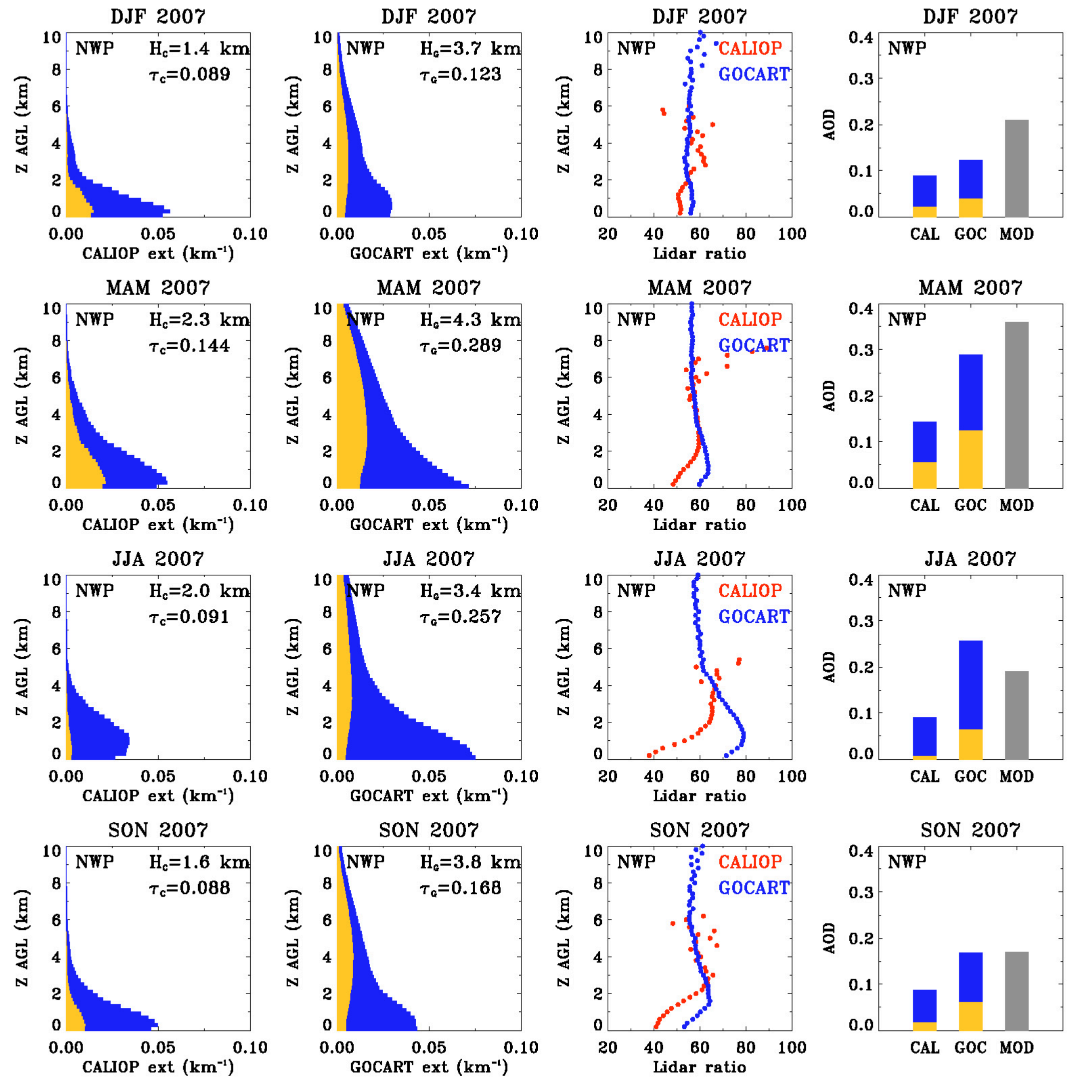

Figure 12: same as Figure 7, but over the northwestern Pacific (NWP).

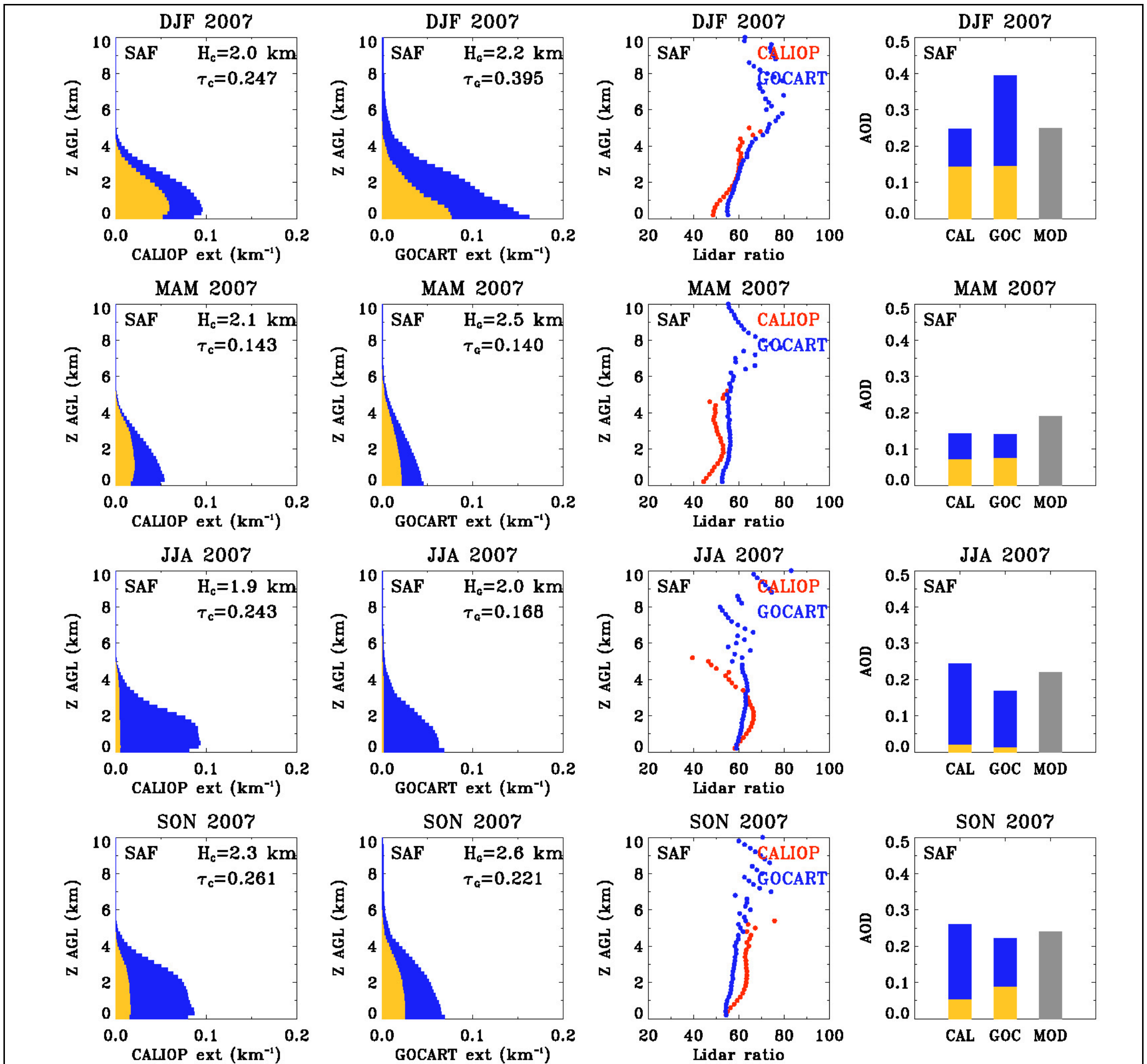

Figure 13: same as Figure 7, but over the southern Africa (SAF).

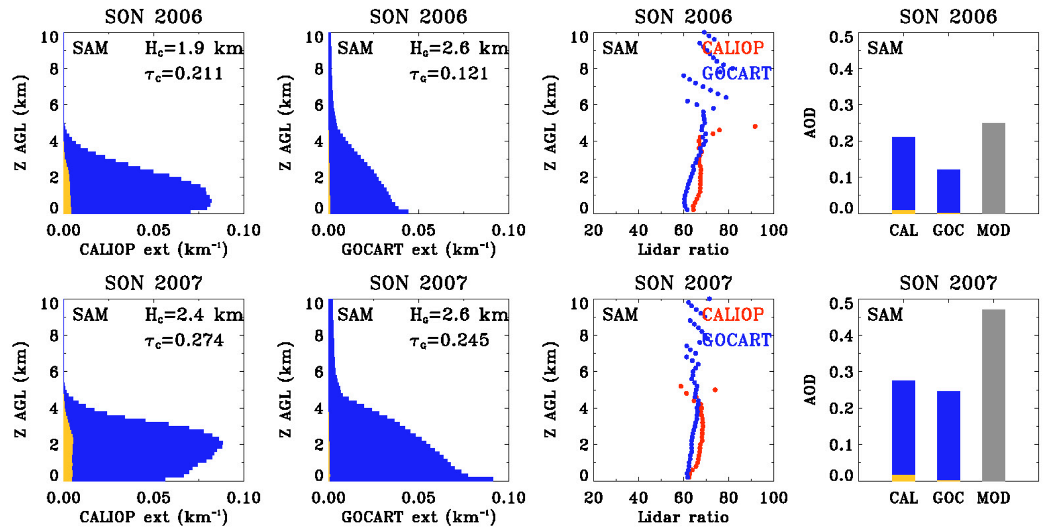

Figure 14: same as Figure 7, but over South America (SAM) and for SON 2006 and SON 2007.

“Global view of aerosol vertical distributions from CALIPSO lidar measurements and GOCART simulations: Regional and seasonal variations”

Hongbin Yu, Mian Chin, David M. Winker, Ali H. Omar, Zhaoyan Liu, Chieko Kittaka, and Thomas Diehl

Online Supplementary Material

The study examines seasonal average extinction profiles, dust and non-dust aerosol separately, over 12 sections representing distinct aerosol regimes, as defined in Figure 2 of the paper. Although similar plots are made for all regions, for conciseness our discussion has been focused on 8 representative regions. This supplementary material collects the similar plots over other 4 regions, namely West Europe (WEU, Figure S1), the western China (WCN, Figure S2), northern Atlantic (NAT, Figure S3), and Southeast Asia (SEA, Figure S4). Table S1 and S2 summarizes comparisons of seasonal and regional average AOD and scale height, respectively, between CALIOP, GOCART, and MODIS over the whole 18-month period (from June 2006 to November 2007) and all 12 sections.

21

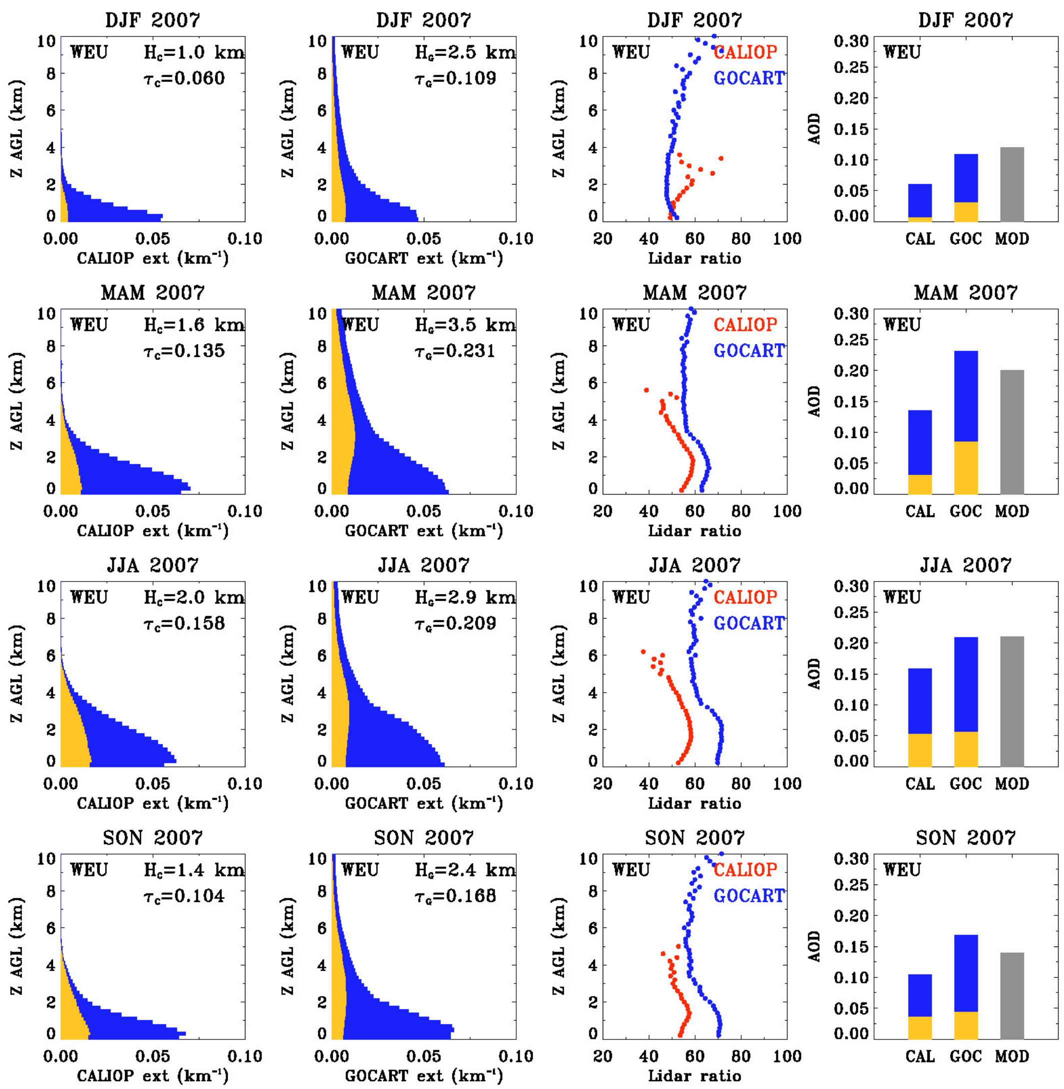

Figure S1: Profiles of seasonal average aerosol extinction coefficient (km^{-1}) and lidar ratio (sr) from CALIOP observation and GOCART model, as well as comparisons of columnar AOD between CALIOP (CAL), GOCART (GOC), and MODIS (MOD) over West Europe (WEU). Values of aerosol scale height (H) and optical depth (τ) are listed in the extinction profile plots, with subscript C and G representing CALIOP and GOCART respectively. Orange and blue shaded area in extinction profile and AOD plots represents contribution of dust and non-dust aerosol, respectively.

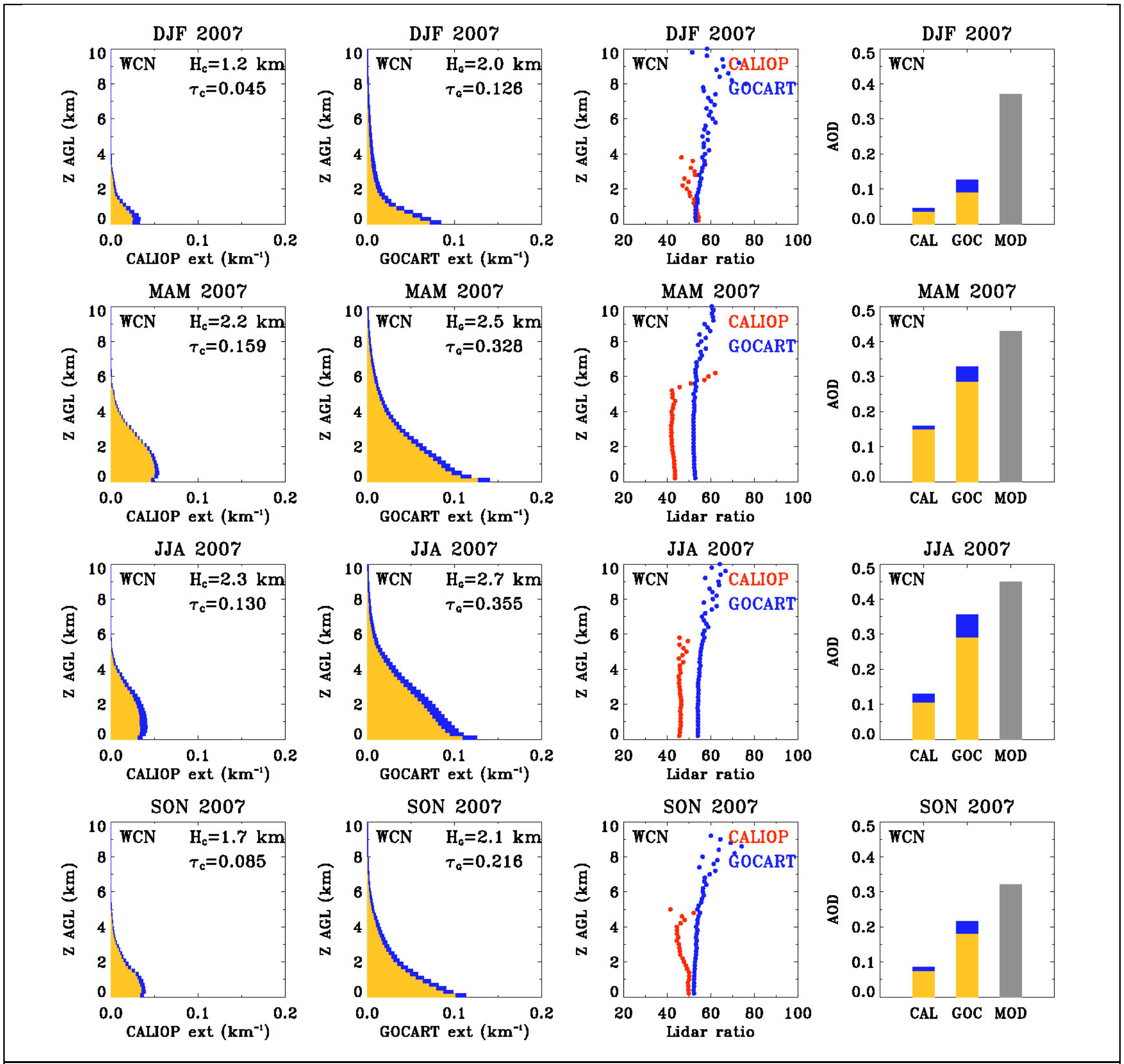

Figure S2: same as Figure S1, but over the western China (WCN). Note that because of missing MODIS retrievals over deserts, MODIS AOD is not directly comparable to CALIOP and GOCART averages.

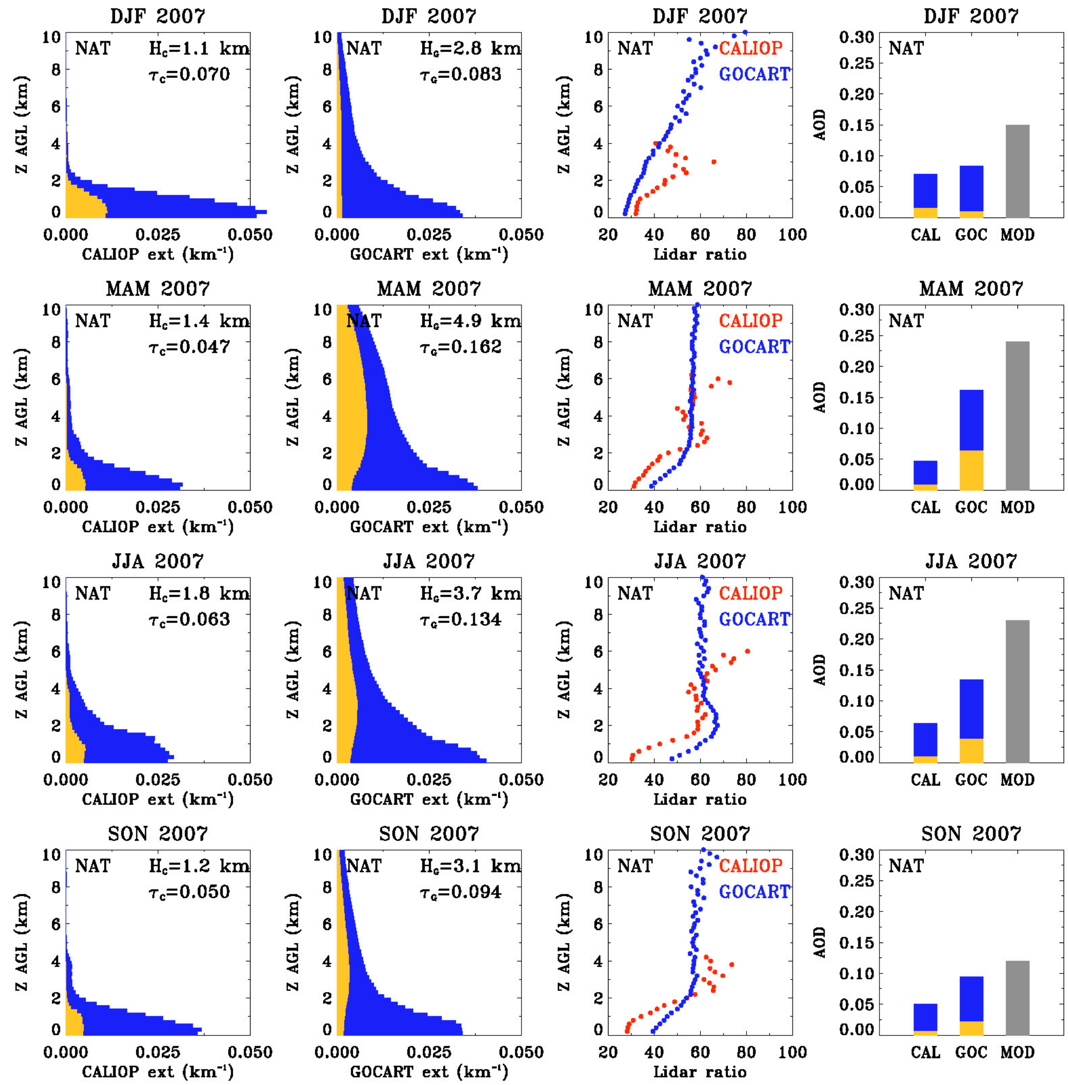

Figure S3: same as Figure S1, but over the northern Atlantic (NAT).

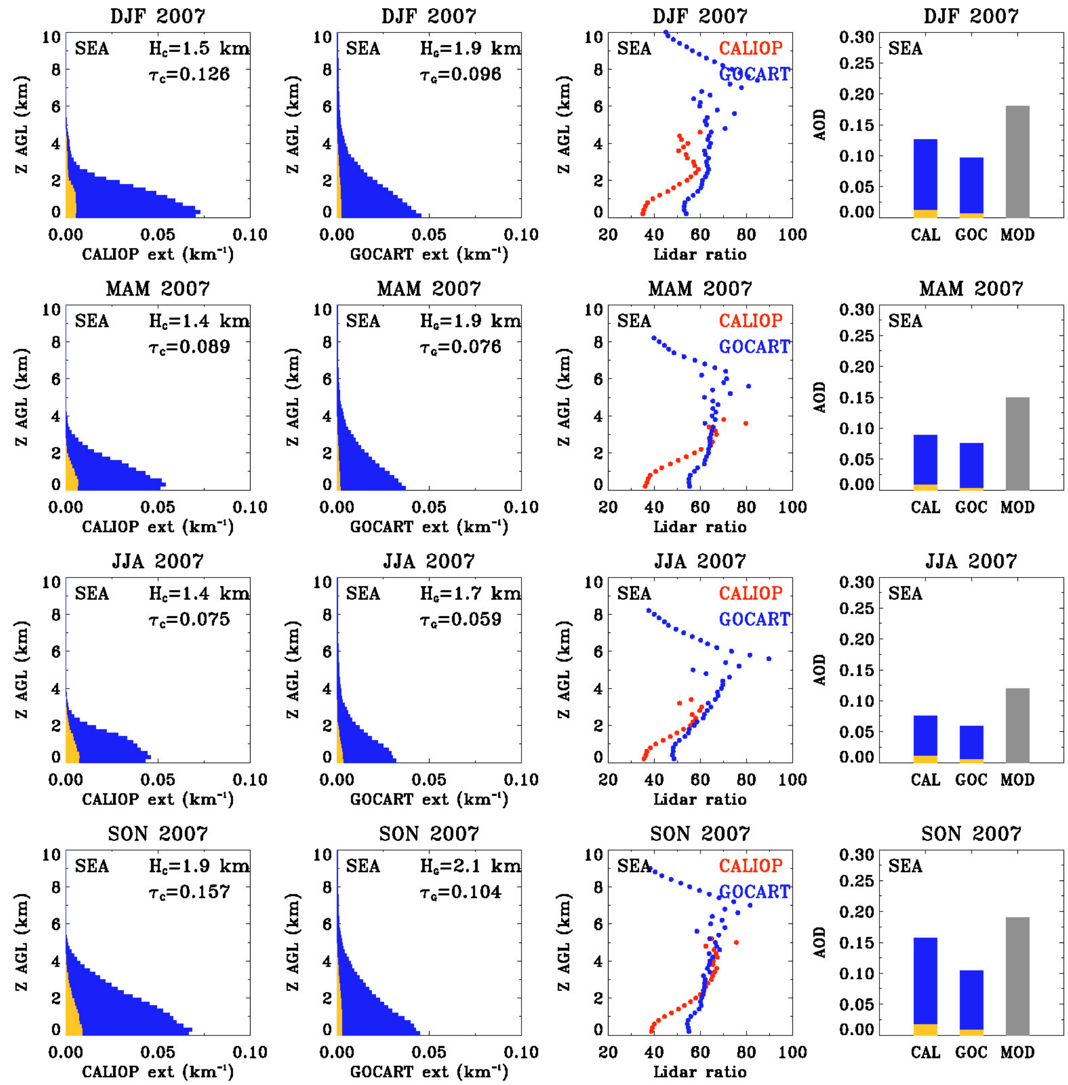

Figure S4: same as Figure S1, but over Southeast Asia (SEA).

Table S1: Seasonal and 18-month average AODs derived from CALIOP, GOCART, and MODIS over the 12 sections. Note that over NAF and WCN, the MODIS numbers are averages over a small portion of the regions because of missing MODIS retrievals over bright deserts and hence is not directly comparable to the CALIOP and GOCART averages.

Regions		JJA 2006	SON 2006	DJF 2007	MAM 2007	JJA 2007	SON 2007	18-month average
EUS	CALIOP	0.16	0.06	0.03	0.10	0.16	0.09	0.10
	GOCART	0.13	0.10	0.06	0.17	0.15	0.11	0.12
	MODIS	0.27	0.10	0.09	0.20	0.28	0.13	0.18
NAT	CALIOP	0.05	0.06	0.07	0.05	0.06	0.05	0.06
	GOCART	0.10	0.09	0.08	0.16	0.13	0.09	0.11
	MODIS	0.16	0.15	0.15	0.24	0.23	0.12	0.18
WEU	CALIOP	0.16	0.10	0.06	0.14	0.16	0.10	0.12
	GOCART	0.22	0.17	0.11	0.23	0.21	0.17	0.18
	MODIS	0.22	0.13	0.12	0.20	0.21	0.14	0.17
IND	CALIOP	0.40	0.37	0.29	0.37	0.33	0.34	0.35
	GOCART	0.27	0.17	0.17	0.23	0.24	0.18	0.21
	MODIS	0.79	0.37	0.34	0.37	0.66	0.37	0.48
ECN	CALIOP	0.26	0.26	0.25	0.26	0.25	0.23	0.25
	GOCART	0.38	0.34	0.23	0.41	0.38	0.29	0.34
	MODIS	0.47	0.45	0.40	0.51	0.48	0.36	0.45
NWP	CALIOP	0.10	0.09	0.09	0.14	0.09	0.09	0.10
	GOCART	0.27	0.16	0.12	0.29	0.26	0.17	0.21
	MODIS	0.22	0.17	0.21	0.36	0.19	0.17	0.22
WCN	CALIOP	0.15	0.10	0.05	0.16	0.13	0.09	0.11
	GOCART	0.30	0.23	0.13	0.33	0.36	0.22	0.26
	MODIS	0.40	0.34	0.37	0.43	0.45	0.32	0.38
NAF	CALIOP	0.30	0.16	0.12	0.23	0.27	0.18	0.21
	GOCART	0.45	0.33	0.34	0.47	0.43	0.47	0.42
	MODIS	0.53	0.28	0.26	0.45	0.46	0.32	0.38
CAT	CALIOP	0.21	0.17	0.19	0.20	0.19	0.17	0.19
	GOCART	0.24	0.16	0.29	0.22	0.21	0.16	0.21
	MODIS	0.34	0.24	0.28	0.35	0.30	0.22	0.28
SAF	CALIOP	0.24	0.24	0.25	0.14	0.24	0.26	0.23
	GOCART	0.18	0.20	0.40	0.14	0.17	0.22	0.22
	MODIS	0.23	0.23	0.25	0.19	0.22	0.24	0.23
SAM	CALIOP	0.11	0.21	0.12	0.03	0.14	0.27	0.15
	GOCART	0.09	0.12	0.12	0.06	0.13	0.25	0.13
	MODIS	0.09	0.25	0.15	0.08	0.12	0.47	0.19
SEA	CALIOP	0.09	0.16	0.13	0.09	0.08	0.16	0.12
	GOCART	0.07	0.16	0.10	0.08	0.06	0.10	0.09
	MODIS	0.14	0.22	0.18	0.15	0.12	0.19	0.17

Table S2: Seasonal average aerosol scale height (km, above ground level) derived from CALIOP and GOCART over the12 sections.

Regions		JJA 2006	SON 2006	DJF 2007	MAM 2007	JJA 2007	SON 2007
EUS	CALIOP	2.0	1.4	1.1	1.8	2.0	1.4
	GOCART	2.7	2.5	3.4	4.2	3.1	2.5
NAT	CALIOP	1.5	1.5	1.1	1.4	1.8	1.2
	GOCART	3.2	3.1	2.8	4.9	3.7	3.1
WEU	CALIOP	2.0	1.3	1.0	1.6	2.0	1.4
	GOCART	2.7	2.3	2.5	3.5	2.9	2.4
IND	CALIOP	2.3	1.6	1.4	2.3	2.1	1.5
	GOCART	2.6	2.0	1.8	2.2	2.4	2.1
ECN	CALIOP	2.0	1.7	1.3	2.0	1.9	1.5
	GOCART	2.4	2.1	2.1	2.8	2.4	2.2
NWP	CALIOP	2.0	1.5	1.4	2.3	2.0	1.6
	GOCART	3.2	3.5	3.7	4.3	3.4	3.8
WCN	CALIOP	2.4	1.9	1.2	2.2	2.3	1.7
	GOCART	2.7	2.2	2.0	2.5	2.7	2.1
NAF	CALIOP	2.8	2.1	1.5	2.4	2.7	2.2
	GOCART	3.0	2.4	1.5	2.6	3.2	2.6
CAT	CALIOP	2.4	1.7	1.3	1.6	2.2	1.6
	GOCART	3.1	2.4	1.7	2.2	3.1	2.5
SAF	CALIOP	2.1	2.1	2.0	2.1	1.9	2.3
	GOCART	2.3	2.2	2.2	2.5	2.0	2.6
SAM	CALIOP	1.7	1.9	1.6	1.4	1.7	2.4
	GOCART	2.4	2.6	2.5	2.1	2.3	2.6
SEA	CALIOP	1.5	1.9	1.5	1.4	1.4	1.9
	GOCART	1.8	2.3	1.9	1.9	1.7	2.1